Cell Metabolism

Article

Overnutrition causes insulin resistance and metabolic disorder through increased sympathetic nervous system activity

Graphical abstract

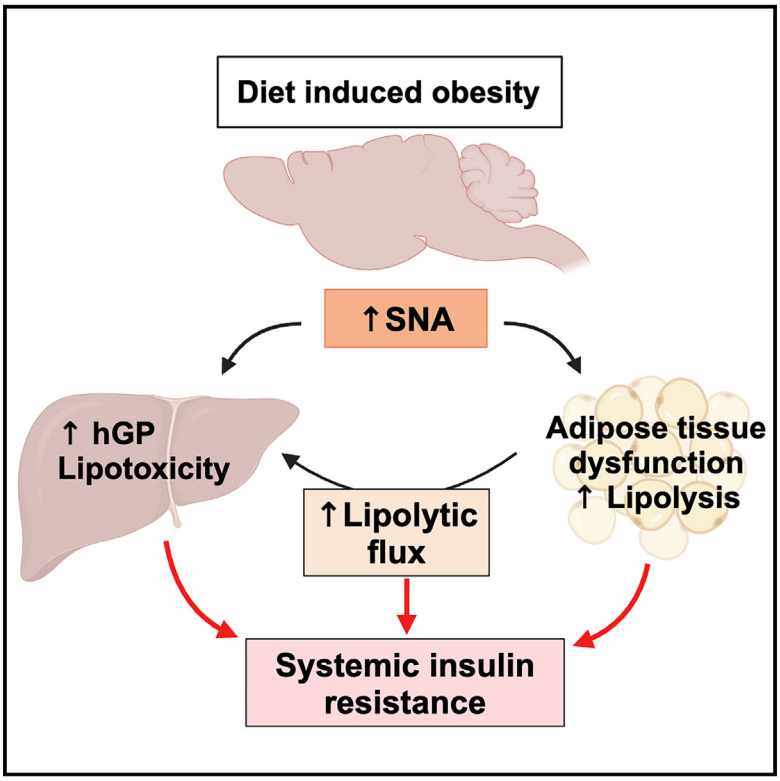

Authors

Kenichi Sakamoto, Mary A. Butera, Chunxue Zhou, ..., Gary J. Schwartz, Azeddine Tahiri, Christoph Buettner

Correspondence

cb1116@rwjms.rutgers.edu

In brief

Sakamoto et al. demonstrate that early overnutrition-induced insulin resistance is due to increased SNS activity (SNA), while cellular insulin signaling is maintained. Elevated SNA drives metabolic disease through increased lipolysis. The findings support a paradigm shift in our understanding of how obesity induces insulin resistance.

Highlights

- HFD feeding rapidly impairs insulin action by increasing SNS activity (SNA)
- Reducing SNA prevents HFD-induced insulin resistance and metabolic disorder
- Early HFD induces insulin resistance before cellular insulin signaling is impaired
- Lipolysis is a key mechanism through which elevated SNA induces insulin resistance

Sakamoto et al., 2025, Cell Metabolism *37*, 1–17
January 7, 2025
https://doi.org/10.1016/j.cmet.2024.09.012

CellPress

Cell Metabolism

CellPress

Article

Overnutrition causes insulin resistance and metabolic disorder through increased sympathetic nervous system activity

Kenichi Sakamoto,[1,2] Mary A. Butera,[1,2] Chunxue Zhou,[2] Giulia Maurizi,[2] Bandy Chen,[1,2] Li Ling,[2] Adham Shawkat,[1] Likhitha Patlolla,[1] Kavira Thakker,[1] Victor Calle,[1] Donald A. Morgan,[3] Kamal Rahmouni,[3] Gary J. Schwartz,[4] Azeddine Tahiri,[1] and Christoph Buettner[1,2,5,*]

[1]Division of Endocrinology, Metabolism & Nutrition, Department of Medicine, Rutgers Robert Wood Johnson Medical School, New Brunswick, NJ, USA

[2]Department of Medicine and Diabetes, Obesity, and Metabolism Institute, Icahn School of Medicine at Mount Sinai, New York, NY, USA

[3]Department of Neuroscience and Pharmacology, Roy J. and Lucille A. Carver College of Medicine, University of Iowa, Iowa City, IA, USA

[4]Department of Medicine & Neuroscience, Albert Einstein College of Medicine, New York, NY, USA

[5]Lead contact

*Correspondence: cb1116@rwjms.rutgers.edu

https://doi.org/10.1016/j.cmet.2024.09.012

SUMMARY

The mechanisms underlying obesity-induced insulin resistance remain incompletely understood, as impaired cellular insulin signaling, traditionally considered the primary driver of insulin resistance, does not always accompany impaired insulin action. Overnutrition rapidly increases plasma norepinephrine (NE), suggesting overactivation of the sympathetic nervous system (SNS). However, the role of the SNS in obesity is controversial, as both increased and decreased SNS activity (SNA) have been reported. Here, we show that reducing catecholamine (CA) release from the SNS protects against overnutrition-induced insulin resistance as well as hyperglucagonemia, adipose tissue dysfunction, and fatty liver disease, as we demonstrate utilizing a mouse model of inducible and peripherally restricted deletion of tyrosine hydroxylase (*th*; THΔper). A key mechanism through which heightened SNA induces insulin resistance is by triggering adipose tissue lipolysis. Increased SNA emerges as a critical driver in the pathogenesis of overnutrition-induced insulin resistance and metabolic disease independent of cellular insulin signaling.

INTRODUCTION

Obesity causes type 2 diabetes and metabolic disease principally through induction of insulin resistance. The risk of developing diabetes is over 3-fold in overweight individuals and more than 10-fold in obese individuals compared with lean individuals.[1] Insulin resistance can rapidly develop during overnutrition even before obesity manifests, resulting in glucose intolerance, adipose tissue dysfunction, and hepatic steatosis. Insulin resistance in adipose tissue is a pivotal contributor to adipose tissue dysfunction, which is characterized by hypertrophic adipocytes,[2] unrestrained lipolysis,[3] reduced lipogenic capacity,[4,5] increased adipose tissue inflammation,[6,7] and fibrosis.[2,7] Insulin resistance in the liver manifests as unrestrained hepatic glucose production (hGP), a key driver of fasting hyperglycemia in diabetes.[8] Hepatic insulin resistance is also believed to contribute to hepatic steatosis that can progress to metabolic dysfunction-associated fatty liver disease (MAFLD). MAFLD is present in more than 70% of all type 2 diabetes cases[9,10] and is the most common reason for fibrosis and liver failure.

The mechanisms of insulin resistance in obesity remain incompletely understood. According to the prevailing paradigm, obesity causes insulin resistance by disrupting intracellular insulin signaling through the canonical insulin receptor-IRS-phosphatidylinositol 3-kinase (PI3K)-AKT-FoxO1 signaling cascade in target tissues such as liver and adipose tissue.[11] However, in the early stages of obesity, cellular insulin signaling appears intact in these tissues, despite the inability of insulin to suppress lipolysis and hGP.[12,13] Hence, impaired cellular insulin signaling in target tissues may not fully account for organismal insulin resistance, defined as reduced suppression of glucose and fatty acids by insulin.

An alternative mechanism contributing to obesity-induced insulin resistance could be heightened counterregulatory signaling resulting from increased sympathetic nervous system (SNS) activity (SNA) and its principal hormone, norepinephrine (NE), which induces adrenergic signaling. The role of the SNS in obesity is controversial, as both increased[14,15] and decreased[16,17] SNA have been reported. These discrepant findings may be attributed to limitations in the methods employed to assess SNA. Studies that directly measure SNA via nerve

Please cite this article in press as: Sakamoto et al., Overnutrition causes insulin resistance and metabolic disorder through increased sympathetic nervous system activity, Cell Metabolism (2024), https://doi.org/10.1016/j.cmet.2024.09.012

recordings, NE turnover, or plasma NE levels frequently report increased SNA in obesity.[18,19] By contrast, studies of adrenergic signaling or effector pathways such as adipose tissue lipolysis[20] often report reduced activation by catecholamine (CA), which is interpreted to reflect reduced SNA in obesity. This paradox may be explained by CA resistance, namely the failure to mount a normal physiological response to CA stimulation due to the reduced expression of the β-adrenergic receptor or adrenergic desensitization, resulting in lower levels of the second messenger cyclic AMP (cAMP).[21,22] CA resistance is commonly observed in obesity[21] and can arise from chronic sympathetic overactivation.[23,24]

While the principal transmitter of the SNS is NE, an integral part of the SNS is the adrenal gland, which releases epinephrine; the SNS also controls glucagon release from the pancreatic α cell.[25] These hormones antagonize insulin action by increasing hGP and inducing lipolysis in adipose tissue.[26] NE has been reported to increase after 4 weeks of high-fat diet (HFD) feeding in mice,[19] a commonly employed model for overfeeding leading to obesity and insulin resistance. The contribution of epinephrine to obesity-induced metabolic disorder is controversial. Although HFD feeding reportedly increases plasma epinephrine in mice,[27] adrenal epinephrine secretion is not increased in obese humans.[28] Well accepted is the role of hyperglucagonemia in obesity-induced insulin resistance, where glucagon secretion is aberrantly increased[29] due to α cell dysfunction, defined as a failure of glucose to suppress glucagon secretion from the pancreatic α cells.[30] It is commonly assumed that α cell dysfunction is mainly due to the failure of β cells to increase insulin secretion when glucose levels rise, as insulin suppresses glucagon secretion from α cells.[30] To what extent increased SNA may contribute to obesity-induced hyperglucagonemia remains unclear.

To delineate the role of the SNS in overnutrition and obesity-induced insulin resistance and metabolic disease, our study initially focused on assessing the impact of overnutrition on SNA and then studied the role of the SNS using a recently developed mouse model of peripherally restricted and inducible deletion of tyrosine hydroxylase (*th*). In these mice, sympathetic CA levels are markedly reduced in peripheral tissues, while central nervous system (CNS) CA levels are maintained. Unlike previous sympathectomy models, this approach avoids potential developmental effects or local inflammation as caused by surgical or chemical sympathectomy. Our findings unveil that overnutrition triggers a surge in SNA, which accounts for the insulin resistance, adipose tissue dysfunction, and hepatic steatosis. A primary mechanism through which increased SNA causes metabolic disease is increased adipose tissue lipolysis, a key target of the SNS.

RESULTS

Short-term overnutrition induces glucose intolerance and insulin resistance and impairs insulin's ability to suppress WAT lipolysis

Male C57BL/6 mice fed an HFD for either 3 or 10 days displayed increased adiposity, even though body weight gain did not reach statistical significance (Figures S1A and S1B). Blood glucose was increased in the fasting and fed state (Figure S1C) despite hyperinsulinemia (Figure S1D). Glucose tolerance and insulin sensitivity were impaired after HFD feeding (Figures S1E and S1F), consistent with insulin resistance, as previously reported.[31,32]

Short-term HFD feeding impaired the ability of insulin to reduce activation of hormone-sensitive lipase (HSL) in epididymal white adipose tissue (eWAT) after HFD feeding (Figures S1G and S1H), indicative of adipose tissue insulin resistance. Consistent with impaired lipolytic regulation, both fasting and random-fed plasma glycerol were elevated following HFD feeding (Figure S1I).

Intriguingly, insulin signaling remained intact in eWAT, liver, and muscle in HFD-fed mice as indicated by comparable induction of the phosphorylation of Akt (Ser 473 and Thr 308) (Figures S2A–S2H). These findings demonstrate that short-term HFD hampers the ability of insulin to inhibit lipolysis in adipose tissue, a key aspect of insulin action in this tissue, even though cellular insulin signaling seems intact.

Activation of HSL, an accepted indicator of SNA of adipose tissue,[33,34] reflects the balance of cellular insulin signaling and cAMP signaling, primarily induced by adrenergic signaling. As cellular insulin signaling was unaltered, increased adrenergic signaling induced by NE may account for the impaired ability of insulin to suppress lipolysis by inhibiting HSL phosphorylation. Plasma NE was increased after short-term HFD (Figure S2I), indicative of an increase in global SNA. Epinephrine, glucagon, and corticosterone were not increased (Figures S2J–S2L), suggesting that increased SNS release of NE may drive adipose tissue lipolysis before hyperglucagonemia develops.

To test whether elevated NE is sufficient to impair glucose homeostasis and adipose tissue function, we infused NE for 14 days subcutaneously, increasing plasma NE levels (Figure S3A). Indeed, NE impaired insulin action (Figures S3B and S3C) and trended to increase HSL phosphorylation without altering body weight, plasma insulin, or basal phosphorylation of Akt (Figures S3D–S3F). NEFA levels were not increased likely due to a compensatory increase in fatty acid utilization (Figure S3G), while acute NE administration robustly increased plasma NEFA levels and the phosphorylation of HSL (Figure S3H, I).

Reduction of CA release from the SNS through peripheral deletion of *th* prevents insulin resistance and glucose intolerance induced by short-term overnutrition

We next examined whether THΔper mice, a mouse model allowing for the inducible and peripherally restricted deletion of *th*,[35] provide protection from HFD-induced metabolic dysfunction. Tamoxifen injection resulted in the deletion of *th* in peripheral tissues including liver, spleen, BAT, eWAT, and inguinal WAT (iWAT), but not in the brain and spinal cord (Figure 1A), due to the peripherally restricted expression of Cre recombinase (Figure 1B). Upon *th* deletion, NE was reduced by more than 90% in peripheral tissues of THΔper mice, while NE levels in the brain were not altered (Figure 1C). Cold tolerance was reduced in THΔper mice fed rodent chow diet (RC), as we reported previously,[35] and also after HFD for 12 weeks (Figures S4A and S4B). Interestingly, while *th* deletion reduces BAT thermogenesis as indicated by the two-way ANOVA genotype effect (p = 0.0001), BAT thermogenesis was significantly lower in the

Please cite this article in press as: Sakamoto et al., Overnutrition causes insulin resistance and metabolic disorder through increased sympathetic nervous system activity, Cell Metabolism (2024), https://doi.org/10.1016/j.cmet.2024.09.012

CellPress

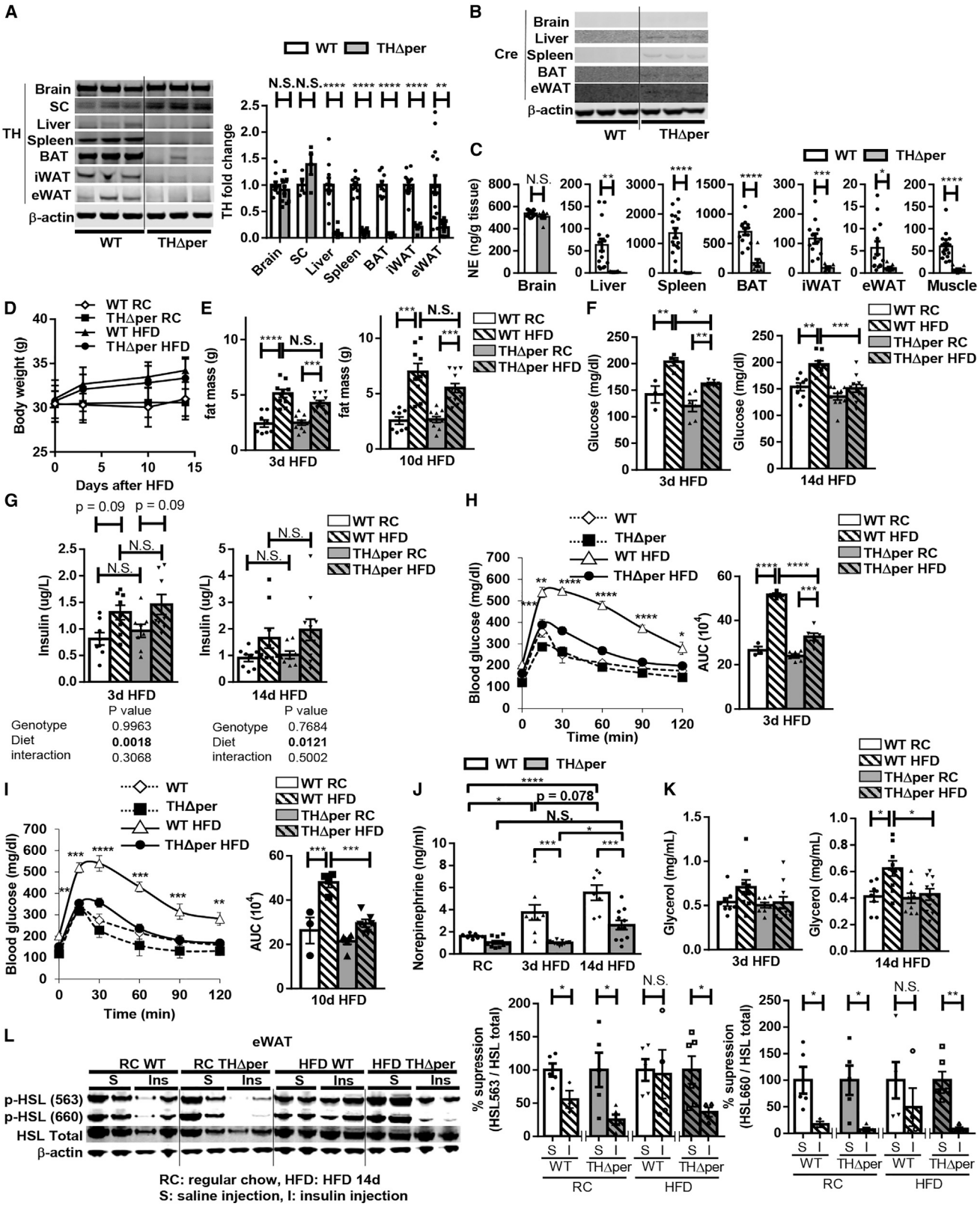

Figure 1. Reduction of SNA through peripheral deletion of *th* prevents glucose intolerance induced by short-term overnutrition

(A) *Th* expression is markedly reduced in peripheral tissues but not in the brain and spinal cord of THΔper mice (n = 4–15).

(B) Cre recombinase protein is expressed only in peripheral tissues but not in the brain of THΔper mice.

(legend continued on next page)

Please cite this article in press as: Sakamoto et al., Overnutrition causes insulin resistance and metabolic disorder through increased sympathetic nervous system activity, Cell Metabolism (2024), https://doi.org/10.1016/j.cmet.2024.09.012

THΔper mice only during RC but not during HFD feeding as assessed through infrared thermal imaging of the BAT region compared with hindquarter region (Figures S4C and S4D). This may be due to impaired BAT thermogenesis after HFD in wild type (WT),[36] which is expected to reduce the difference in BAT thermogenesis. Nevertheless, the body core temperature of THΔper mice at room temperature was comparable to that of WT mice, demonstrating that these mice are able to maintain thermogenesis at room temperature.

Further confirmation of reduction of SNA was obtained by studying counterregulation after administration of 2-deoxy-D-glucose (2-DG), which increases SNA and secretion of counterregulatory hormones by inducing neuroglycopenia. THΔper mice exhibited impaired counterregulation with lower glucose excursions and reduced CA and glucagon levels (Figures S4E and S4F). Gene expression of *npy*, a sympathetic cotransmitter, was comparable in the eWAT of both THΔper mice and WT mice (Figure S4G), suggesting that *npy* expression in sympathetic nerve fibers is unaffected by the *th* deletion. Hence, THΔper mice serve as a valuable pharmacogenetic model to test the role of sympathetically released CA and increased SNA.

14 days of HFD-increased body weight and adiposity equally in THΔper and WT mice (Figures 1D and 1E) with lean mass unaltered (Figure S4H). Overnutrition-induced increases in fasting glycemia were prevented in THΔper mice (Figure 1F) with comparable fasting insulin levels (Figure 1G). Moreover, the overnutrition-induced glucose intolerance after 3 or 10 days of HFD feeding was profoundly improved in THΔper mice feeding (Figures 1H and 1I), coinciding with a blunted increase in NE levels in the HFD-fed THΔper mice (Figure 1J). Notably, while HFD feeding up to 14 days did not increase fasting epinephrine and glucagon in WT mice, epinephrine and glucagon were significantly lower in THΔper mice fed either RC or HFD (Figure S4I).

Surprisingly, even though the SNS is a key driver of lipolysis,[37] neither NEFA nor glycerol levels were lower in THΔper mice fed RC, suggesting the presence of a compensatory mechanism that maintains normal NEFA and glycerol levels even in the setting of profoundly reduced adrenergic signaling (Figures 1K and S4J). By contrast, the increase in fasting plasma glycerol after 14 days of HFD feeding was markedly reduced in THΔper mice (Figure 1K), consistent with the improved ability of insulin to reduce HSL phosphorylation after overnutrition in THΔper mice (Figure 1L). These results demonstrated that increased lipolysis induced by overnutrition is ameliorated in THΔper mice.

Insulin-induced phosphorylation of the insulin receptor (liver, eWAT), Akt (liver, eWAT, iWAT), and glycogen synthase kinase-3 beta (GSK3β) (liver) were similar in both THΔper mice and WT mice fed RC and HFD compared with saline-injected controls (Figures S5A–S5C). This indicates that the metabolic improvement in the THΔper occurs independent of alterations in cellular insulin signaling. Taken together, these results demonstrate that preventing an increase in SNS outflow and adrenergic signaling ameliorates the glucose intolerance and restores insulin action in adipose tissue without affecting cellular insulin signaling in a mouse model of short-term overnutrition.

Reduction of SNA improves long-term HFD feeding-induced glucose intolerance

After 10 weeks of HFD feeding, THΔper mice continued to exhibit comparable weight gain, food intake, and body composition compared with WT littermates (Figures 2A–2C), indicating that the metabolic protection conferred by a reduction of SNA during long-term HFD feeding occurred independent of differences in body weight, food intake, or adiposity.

While insulin levels were comparable after 12 weeks of HFD feeding, glucose tolerance was markedly improved in the THΔper mice (Figures 2D and 2E), with similar glucose excursion between the HFD-fed THΔper mice and those of RC-fed WT mice, suggesting that impaired insulin action was improved in THΔper mice.

Insulin signaling in liver, eWAT, and muscle was comparable in THΔper and WT mice fed either RC (Figures 2F–2I) or HFD for 12 weeks (Figures 2F and 2J–2L). Plasma NEFA and glycerol were lower in the THΔper mice fed HFD (Figure 2M), consistent with protection against a rise in lipolysis despite comparable gain in adiposity. To confirm that diet-induced obesity increases SNA, we performed nerve recording studies. These demonstrated that SNA is elevated in both eWAT and iWAT after 16 weeks of HFD feeding (Figure 2N). Furthermore, THΔper mice were protected from the 12 weeks of HFD-induced increases in NE, epinephrine, and glucagon (Figure 2O), indicating that the increase of these counterregulatory hormones in the setting of obesity is largely due to increased SNA and sympathetically released CA. Of note, corticosterone, which is under the control of the hypothalamic-pituitary-adrenal (HPA) axis, was not different between WT and THΔper mice (Figure 2O).

Reducing sympathetic activation ameliorates HFD-induced hepatic insulin resistance

We assessed hepatic insulin action in THΔper and WT mice fed with HFD for 16 weeks by performing hyperinsulinemic-euglycemic clamps combined with tracer dilution technique (Figure 3A). Throughout the clamp, euglycemia was similarly maintained in the THΔper and WT mice (Figure 3B), and there was a comparable increase in plasma insulin in the two strains (Figure 3C), while plasma glucagon levels were lower in THΔper mice (Figure 3D).

(C) NE is markedly reduced in peripheral tissues but not in the brain of THΔper (n = 6–17).
(D) Body weight of THΔper mice and WT mice fed RC or HFD (n = 8–11).
(E) Fat mass of THΔper mice and WT mice fed RC or HFD for 3 or 10 days (n = 8–11).
(F and G) Fasting plasma glucose (F) and insulin (G) of THΔper mice and WT mice fed RC or HFD for 3 or 14 days (n = 8–11).
(H and I) Glucose tolerance of THΔper mice and WT mice fed RC or HFD for 3 (H) or 10 days (I) (n = 3–6). Right: AUC of blood glucose.
(J) Plasma NE of THΔper mice and WT mice fed RC or HFD (n = 7–11).
(K) Plasma glycerol of THΔper mice and WT mice fed RC or HFD for 3 or 14 days (n = 8–10).
(L) Insulin's impaired ability to reduce phosphorylation of HSL is ameliorated in eWAT of THΔper mice after 14 days of HFD feeding (n = 3–6).
Data are expressed as the mean ± SEM. $^{*}p < 0.05$; $^{**}p < 0.01$; $^{***}p < 0.001$; $^{****}p < 0.0001$; according to a two-sided Student's t test (H and I: * mean $p < 0.05$ vs. THΔper fed HFD) or two-way ANOVA with Tukey's test. AUC, area under the curve; SC, spinal cord.
See also Figures S1–S5.

Please cite this article in press as: Sakamoto et al., Overnutrition causes insulin resistance and metabolic disorder through increased sympathetic nervous system activity, Cell Metabolism (2024), https://doi.org/10.1016/j.cmet.2024.09.012

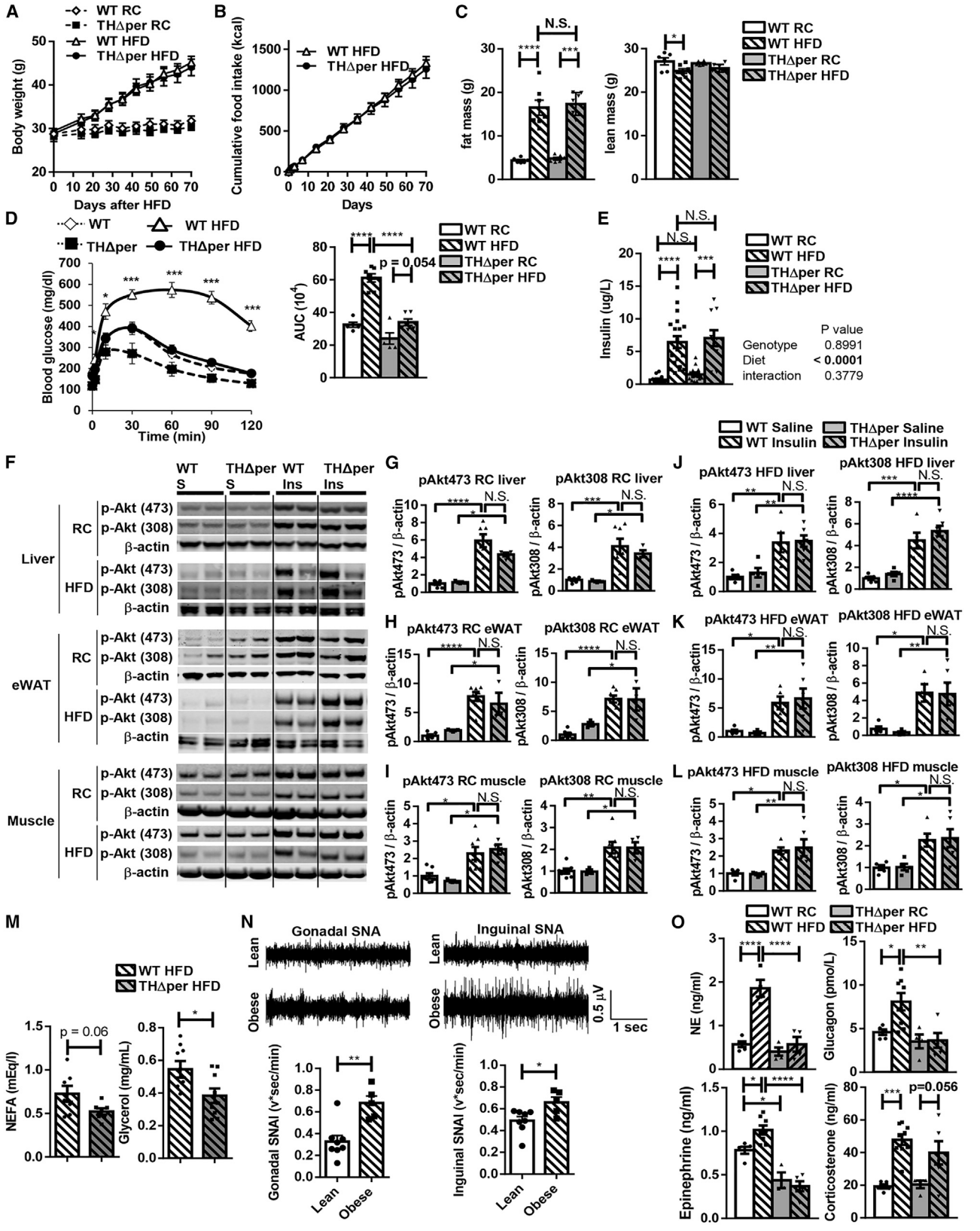

(legend on next page)

Please cite this article in press as: Sakamoto et al., Overnutrition causes insulin resistance and metabolic disorder through increased sympathetic nervous system activity, Cell Metabolism (2024), https://doi.org/10.1016/j.cmet.2024.09.012

The glucose infusion rate (GIR) required to maintain euglycemia was significantly higher in THΔper mice (Figure 3E), indicating an improvement in the HFD-induced insulin resistance. Notably, the ability of insulin to suppress hGP was markedly improved in THΔper mice (Figures 3F and 3G), whereas basal hGP was not reduced. The increase in the glucose utilization rate, as assessed by the glucose disposal rate (Rd), was comparable in both groups (Figure 3H), suggesting that the SNS is not a major regulator of peripheral glucose utilization during hyperinsulinemia and in the setting of chronic HFD feeding.

Despite markedly improved hepatic insulin action, hepatic insulin signaling was similar in THΔper and WT mice at the conclusion of the hyperinsulinemic clamp (Figures 3I and 3J). Of note, the degree of hyperinsulinemia induced during the clamp was within a physiological range (Figure 3C), allowing for the examination of insulin signaling during physiological hyperinsulinemia. Insulin signaling and phosphorylation of phosphodiesterase 3B (PDE3B) were not different in eWAT of THΔper mice compared with WT (Figures 3K and 3L). However, the ability of insulin to suppress phosphorylation of HSL and perilipin as well as activation of protein kinase A (PKA) was markedly improved in eWAT during the hyperinsulinemic clamp study (Figures 3K, 3M, and 3N), consistent with improved adipose tissue insulin action reduced fasting NEFA and glycerol in THΔper mice fed HFD (Figures 2M and 3O). These results support the notion that increased SNA, rather than reduced cellular insulin signaling, accounts for the insulin resistance in chronic obesity.

Reducing sympathetic activity ameliorates adipose tissue dysfunction

We next examined the role of the SNS in obesity-induced adipose tissue dysfunction, characterized by reduced lipogenic capacity,[4] adipocyte hypertrophy,[2] unrestrained lipolysis,[3,12,38] metabolic inflammation,[6] fibrosis, and senescence.[39] To assess *de novo* lipogenesis (DNL), we examined the protein and mRNA expression of key DNL enzymes such as fatty acid synthase (FAS), ATP-citrate lyase (ATPCL), and acetyl-coenzyme A (CoA) carboxylase (ACC) and phosphorylation of ATPCL. Suppression of DNL in eWAT after HFD feeding was prevented in THΔper mice (Figures 4A, 4B, and S6A), which was also reflected in a marked increase in the insulin-sensitizing lipokine C16:1-palmitoleate, which is produced by DNL in WAT[40] (Figure 4C).

Interestingly, basal phosphorylation of HSL and perilipin was markedly reduced after HFD feeding (Figures 4A and 4D), possibly due to chronic overstimulation and CA resistance.[17] Increased adipocyte size is commonly associated with insulin resistance in obesity and inversely correlates with metabolic health,[2] while a higher number of small adipocytes, indicative of higher adipogenesis rates, is often associated with a metabolically healthier phenotype in individuals[41] and rodents[42] with obesity. Notably, THΔper mice exhibited reduced adipocyte area, diameter, and volume in eWAT after 16 weeks of HFD feeding, while the weight of eWAT remained comparable, consistent with an increase in the number of smaller adipocytes in the THΔper mice (Figures 4E–4G and S6B). Additionally, the HFD-induced suppression of genes that are upregulated during adipogenesis, such as *pparg* and *cebpa*, was ameliorated in THΔper mice (Figure S6C), consistent with the increased number of smaller adipocytes in THΔper mice.

Adipose tissue inflammation after HFD feeding was ameliorated in THΔper mice, as illustrated by the reduced number of crown-like structures composed of macrophages surrounding dead or dying adipocytes and lower mRNA levels of inflammatory cytokines (*ccl2* and *tnfa*) and macrophage markers (*f4/80*, *cd11c*, and *cd68*) (Figures 4H and 4I). Expression of fibrosis-related genes such as fibronectin1 (*fn1*), collagen 16a1 (*col16a1*), *itgb2*, matrix metalloproteinase12 (*mmp12*), *mmp19*, *pcolce2*, *acta2*, and *tgfb* was ameliorated in THΔper mice (Figure S6D). Adipose tissue fibrosis is believed to arise from hypoxia due to the expansion of adipose tissue and ensuing induction of the hypoxia-inducible factor 1-alpha (*hif1a*).[2] Indeed, HFD-induced *hif1a* expression was ameliorated in the THΔper mice (Figure S6D). Masson's trichrome staining of fibrillar collagen I and III demonstrated that HFD led to the development of thick collagen sheets consistent with fibrosis, which was ameliorated in THΔper mice (Figure 4J). This indicates that adipose tissue fibrosis occurs independent of adipose tissue mass but is a consequence of increased SNA. Finally, THΔper mice were protected from an increase in the expression of senescence markers such as *gpnmb*,[43] *cdkn1a*, and *cdkn2a* after HFD feeding in eWAT (Figure 4K). In summary, these results provide strong evidence that increased SNA is a key driver of multiple aspects of obesity-induced adipose tissue dysfunction.

Reducing SNA ameliorates HFD-induced fatty liver

MAFLD is a common hepatic manifestation of metabolic disease. Impaired lipid metabolism is believed to be a key driver of fatty liver. Given that THΔper mice exhibit markedly improved adipose tissue function and lipid metabolism, we next tested whether a suppression of SNA protects from HFD-induced

Figure 2. Reduction of SNA through peripheral deletion of *th* improves long-term HFD feeding-induced glucose intolerance

(A) Body weight of THΔper mice and WT mice fed RC (n = 4–5) or HFD (n = 9–13).

(B) Food intake of THΔper mice and WT mice fed HFD (n = 5–7).

(C) Fat mass and lean mass of THΔper mice and WT mice fed RC or HFD (n = 6–7).

(D) Glucose tolerance of THΔper mice and WT mice fed RC or HFD for 12 weeks (n = 5–7). Right: AUC of blood glucose.

(E) Fasting plasma insulin of THΔper mice and WT mice fed RC or HFD for 12 weeks (n = 10–19).

(F–L) Insulin-induced phosphorylation of Akt in liver (G and J), eWAT (H and K), and muscle (I and L) displayed similar increases in both THΔper mice and WT mice fed RC or HFD (n = 3–7).

(M) Plasma NEFA and glycerol of THΔper mice and WT mice fed HFD for 12 weeks (n = 7–9).

(N) Direct multiunit recordings of gonadal and inguinal SNA were obtained in mice fed RC (lean) or 16 weeks of HFD (obese). Segments of original records of baseline SNA and average data are shown (n = 5–8).

(O) Plasma NE (n = 4–5), epinephrine (n = 3–8), glucagon (n = 4–8), and corticosterone (n = 4–9) of THΔper mice and WT mice fed RC or HFD for 12 weeks.

Data are expressed as the mean ± SEM. *$p < 0.05$; **$p < 0.01$; ***$p < 0.001$; ****$p < 0.0001$; according to a two-sided Student's t test (D: * mean $p < 0.05$ vs. THΔper fed HFD) or two-way ANOVA with Tukey's test.

Please cite this article in press as: Sakamoto et al., Overnutrition causes insulin resistance and metabolic disorder through increased sympathetic nervous system activity, Cell Metabolism (2024), https://doi.org/10.1016/j.cmet.2024.09.012

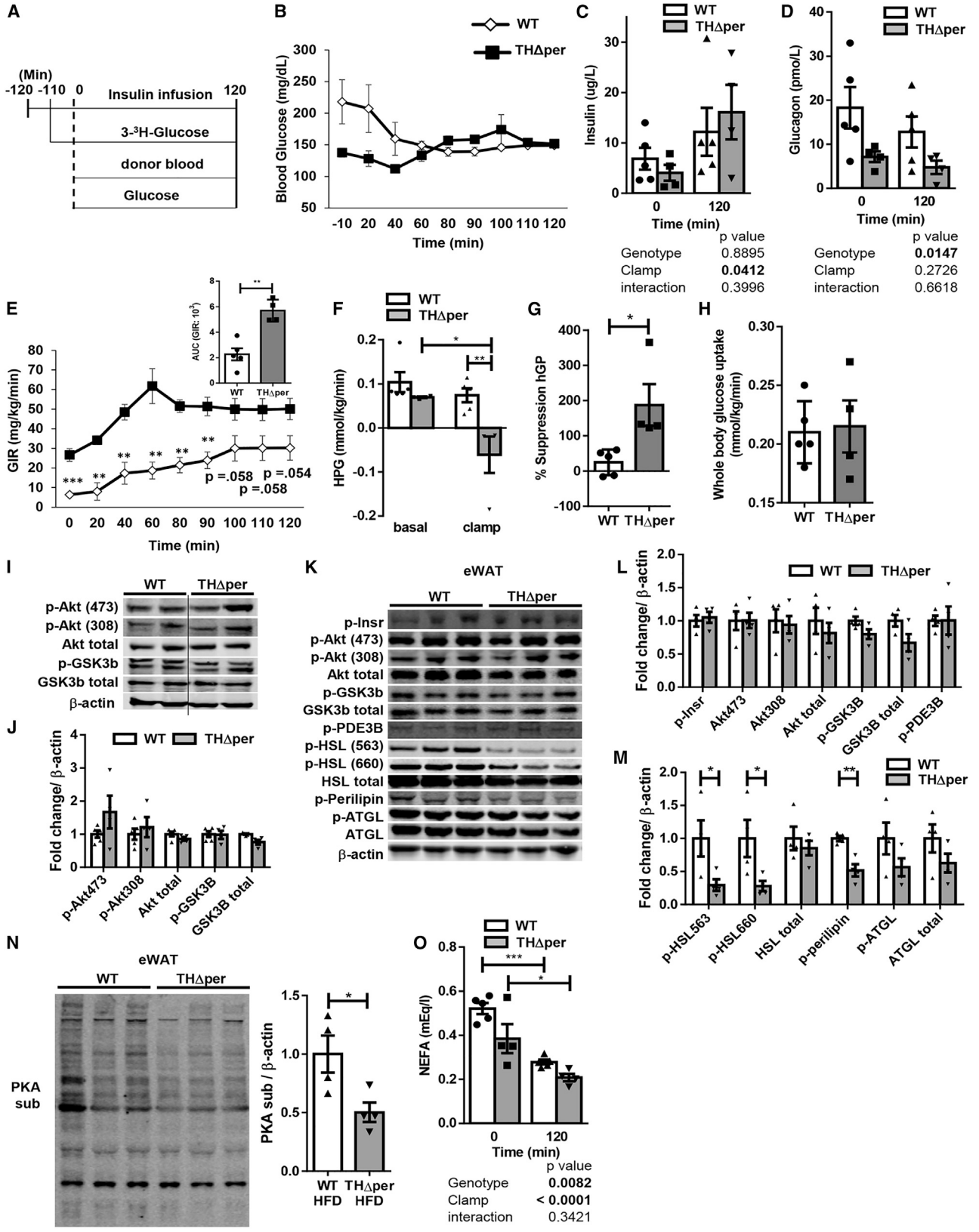

(legend on next page)

hepatic steatosis. H&E staining revealed the presence of hepatic steatosis after 16 weeks of HFD feeding (Figure 5A). This observation was further confirmed by oil red O staining (Figures 5B and 5C) and biochemical quantification of triglyceride (TG) content after Folch extraction (Figure 5D). Importantly, hepatic steatosis was significantly alleviated in THΔper mice.

A contributor to hepatic steatosis is increased hepatic lipogenesis, in part through increased expression of DNL enzymes (FAS, ATPCL, and ACC). HFD feeding significantly increased FAS, phosphorylation of ACC, and phosphorylation of ATPCL (Figures 5E and 5F). Phosphorylation of ACC and ATPCL were decreased in THΔper mice compared with WT mice fed an HFD, indicating reduced lipid biosynthesis in the livers of THΔper mice. The fatty acid transport protein CD36 facilitates fatty acid uptake from plasma into the liver and can contribute to hepatic steatosis.[44] HFD-induced CD36 overexpression was attenuated in THΔper mice (Figures 5E and 5G), suggesting that THΔper mice may be protected from hepatic steatosis in part through decreased lipid uptake into the liver.

Within hepatocytes, glycerol kinase (GK) phosphorylates glycerol into glycerol-3-phosphate, which is a substrate for TG synthesis or gluconeogenesis.[45] The HFD-induced increase in GK protein expression was ameliorated in THΔper mice (Figures 5E and 5G), which may contribute to the reduced hGP and hepatic lipid accumulation. HFD-increased mRNA expression of aquaglyceroporin3 (*aqp3*) and *aqp9*, which facilitate glycerol uptake by the liver, and several enzymes that participate in TG synthesis, including *gk*, glycerol-3-phosphate acyltransferase (GPAT1, encoded by *gpam*), diacylglycerol acyltransferase 1 (*dgat1*), and monoacylglycerol acyltransferase 1 (*mogat1*), were ameliorated in THΔper mice (Figure 5H).

Steatosis is a precursor to steatohepatitis primarily through inflammation. Notably, the induction of phosphorylated nuclear factor κB (NF-κB) and IκB after HFD feeding was prevented in the THΔper mice (Figures 5E and 5G). HFD-induced mRNA induction of inflammatory markers associated with steatohepatitis such as macrophage inflammatory protein 2 (*mip2*); chemokines interferon gamma-induced protein 10 (*ip10*), interleukin-1α (*il1a*), interleukin-1β (*il1b*), and *tnfa*; and macrophage markers (*f4/80* and *cd68*) were substantially reduced in THΔper mice (Figure 5I).

Considering that inflammation associated with MAFLD contributes to hepatic fibrosis, we assessed hepatic expression of fibrosis-related genes (*col3a1*, *col4a1*, *col5a1*, *col5a2*, *col6a1*, *col14a1*, *col16a1*, *fn1*, *lgals3*, *loxl2*, *pcolce*, and *acta2*) and tissue matrix remodeling components (*mmp2*, *mmp19*, and *timp1*). HFD feeding resulted in an increase in mRNA levels of fibrosis markers, which was mitigated in THΔper mice (Figure 5J), suggesting a key role of increased SNA in driving hepatic fibrosis development. Collectively, these findings underscore that the prevention of excessive SNA in obesity results in a comprehensive improvement of hepatic metabolism encompassing a reduction in steatosis and restrained hGP, along with reduced inflammation and possibly a reduced risk of fibrosis development.

Reducing sympathetic activation ameliorates HFD-induced CA resistance

On a cellular level, CA resistance manifests as reduced β-adrenergic signaling due to reduced expression of the β-adrenergic receptor (Adrb),[20,46] lower cAMP signaling in response to β-agonists, and consequently a decrease in CA-induced lipolysis in adipose tissue. Long-term HFD suppressed protein expression and phosphorylation of HSL (Figure 4D), which may be due to CA resistance induced by chronic SNS overdrive, as SNA to adipose tissue (Figure 2N) and plasma NE levels (Figure 2O) continue to be high after long-term HFD. Hence, we assessed CA resistance by administering the β3 agonist CL 316,243 (CL). CL raised plasma NEFA levels, and this response was markedly impaired in mice fed long-term HFD (12 weeks), while those on short-term (3 weeks) HFD showed no such impairment (Figures 6A and 6B), demonstrating that CA resistance is induced only after long-term HFD feeding. The compromised physiological response to adrenergic stimulation after HFD feeding was ameliorated in the THΔper mice as evidenced by a trend toward increased NEFA levels after CL (Figure 6C) and improved HSL activation in eWAT in THΔper mice (Figure 6D). This improvement can be attributed to the maintenance of mRNA expression of Adrb3 (Figure 6E). These results suggest that THΔper mice are protected from CA resistance likely due to reduced chronic sympathetic stimulation.

Adipose tissue lipolysis is required for SNA-induced glucose intolerance

A key role of the SNS is to stimulate lipolysis in adipose tissue. Unrestrained adipose tissue lipolysis due to elevated SNA may contribute to insulin resistance by providing the gluconeogenic precursor glycerol[47] and NEFA, which support increased hGP. Here, we tested whether lipolysis is required for the SNA-induced insulin resistance. We found that administration of NE robustly impaired insulin action (Figures 7A and 7B), but the

Figure 3. Reducing sympathetic activation ameliorates HFD-induced insulin resistance

(A) Schematic representation of hyperinsulinemic-euglycemic clamp protocol. THΔper mice (n = 4) and WT mice (n = 5).
(B) Blood glucose of THΔper mice and WT mice fed HFD for 16 weeks during hyperinsulinemic clamps.
(C and D) Plasma insulin (C) and glucagon (D) during the basal and hyperinsulinemic clamp period.
(E) GIR required to maintain euglycemia during the hyperinsulinemic clamps is higher in THΔper mice. Upper right: AUC of GIR.
(F) hGP during basal and clamp periods. The ability of insulin to suppress hGP was markedly improved in THΔper mice.
(G) Percentage suppression of hGP.
(H) The increase in the glucose utilization rate was comparable in THΔper mice and WT mice during the hyperinsulinemic phase.
(I and J) Phosphorylation of Akt and GSK3β in liver was comparable in THΔper mice and WT mice during the hyperinsulinemic phase.
(K and L) Phosphorylation of insulin receptor (Insr), Akt, GSK3β, and PDE3B in eWAT was comparable in THΔper mice and WT mice during the hyperinsulinemic phase.
(M and N) The ability of insulin to suppress activity of HSL, perilipin (M), and PKA (N) in eWAT is improved in THΔper mice.
(O) Plasma NEFA during the basal and hyperinsulinemic clamp periods.
Data are expressed as the mean ± SEM. *$p < 0.05$; **$p < 0.01$; ***$p < 0.001$; according to a two-sided Student's t test.

Please cite this article in press as: Sakamoto et al., Overnutrition causes insulin resistance and metabolic disorder through increased sympathetic nervous system activity, Cell Metabolism (2024), https://doi.org/10.1016/j.cmet.2024.09.012

CellPress

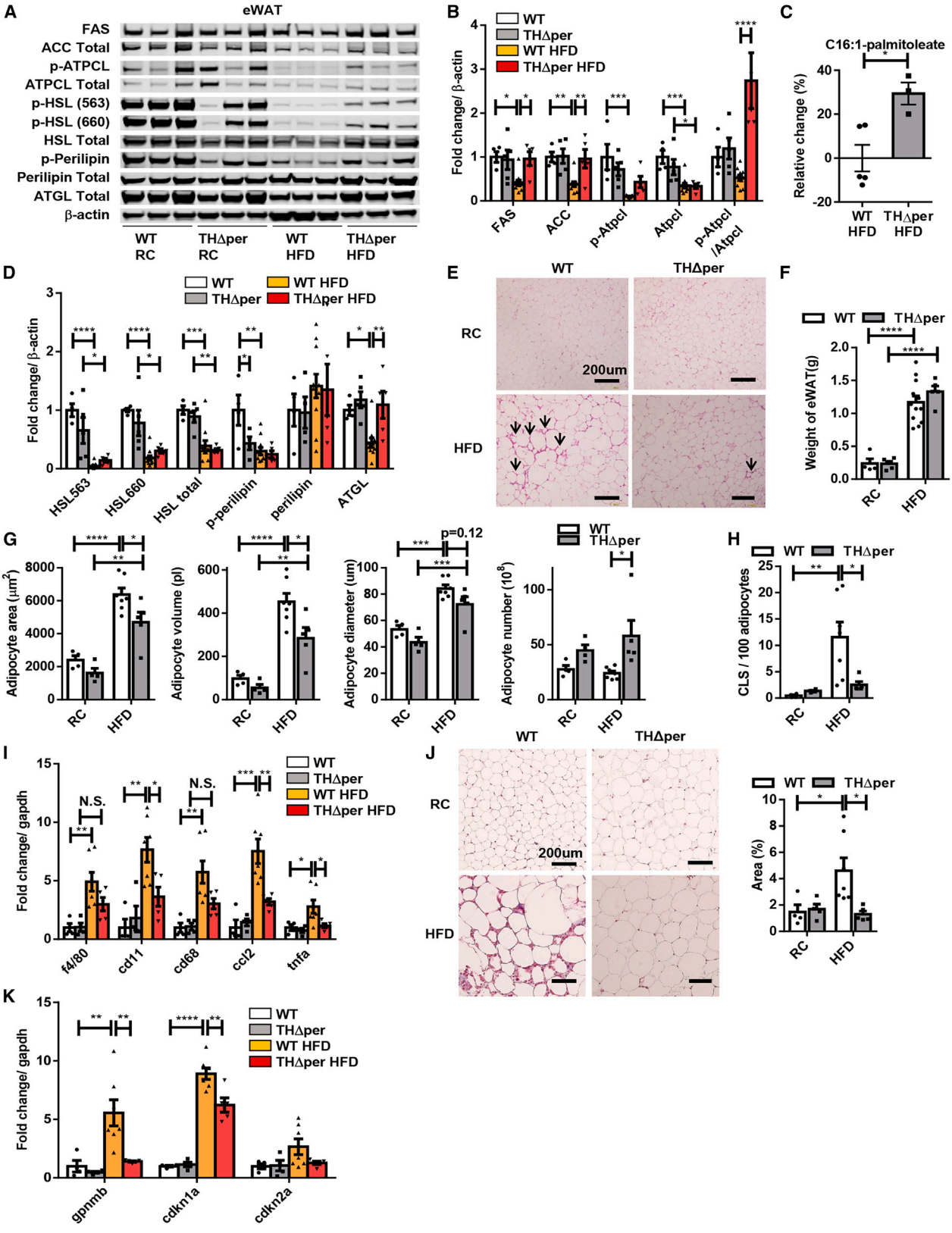

(legend on next page)

impairment was reversed upon pharmacological inhibition of lipolysis by oral administration of the adipose triglyceride lipase (ATGL) inhibitor ATGListatin (Figures 7A–7C).[48] We next tested the role of adipose tissue lipolysis in obesity-induced insulin resistance by using mice that carry an adipose tissue-specific deletion of ATGL (AAKO) and feeding them an HFD for 28 days. AAKO mice exhibited markedly reduced *atgl* expression in eWAT (Figure 7D), comparable weight gain, adiposity, and food intake as WT controls (Figures 7E and 7F), but were protected from HFD-induced insulin resistance (Figure 7G), consistent with a previous report.[49] AAKO mice exhibited reduced plasma NEFA levels (Figure 7H), reduced mRNA levels of inflammatory cytokines as well as macrophage markers (Figure 7I), and lower liver TG content (Figure 7J). These studies indicate that SNA overdrive is sufficient to induce insulin resistance and that the SNS-induced insulin resistance requires lipolysis. Likewise, lipolysis is required for HFD-induced insulin resistance.

DISCUSSION

Here, we investigated mechanisms underlying overnutrition-induced insulin resistance, specifically the role of the SNS and CA using THΔper mice, a mouse model of peripherally restricted CA deficiency that allows to study the role of CA released from the SNS. Our studies led to four key findings. First, overnutrition leads to a rapid impairment of insulin action along with increased SNA and adipose tissue lipolysis despite intact cellular insulin signaling. Second, THΔper mice are protected from HFD-induced glucose intolerance and insulin resistance and maintain hepatic insulin sensitivity despite comparable weight and adiposity gain, food intake, and cellular insulin signaling. Third, THΔper mice are protected from key manifestations of HFD-induced metabolic disease, including adipose tissue dysfunction and fatty liver. Fourth, increased adipose tissue lipolysis is a key mechanism through which increased SNA induces insulin resistance. These findings demonstrate that increased SNS outflow is a key driver of insulin resistance and metabolic disease in diet-induced obesity.

Our studies in the THΔper mice revealed that increased SNA drives insulin resistance independently of changes in cellular insulin signaling during both short-term and long-term HFD feeding. While impairment in cellular insulin signaling is commonly deemed the principal driver of insulin resistance, previous studies reported both impaired[50] and intact[51] cellular insulin as assessed through Akt phosphorylation in liver, adipose tissue, and skeletal muscle after HFD feeding, suggesting that impaired cellular insulin signaling may not always or fully account for insulin resistance. Here, we examined insulin signaling in the setting of HFD feeding after acute and maximal insulin stimulation, as well as after the induction of physiological hyperinsulinemia. Both approaches did not reveal differences in cellular insulin signaling between THΔper and WT mice, suggesting that the marked improvement of hepatic insulin action in the THΔper mice after HFD feeding is not due to enhanced cellular insulin signaling but rather due to the attenuation of increased SNA.

This study provides important insights into the key role of the SNS in driving the dysregulation of counterregulatory hormones in obesity-induced insulin resistance. The finding that reducing CA release from the SNS prevents the obesity-induced hyperglucagonemia suggests that inappropriate SNA is a key culprit of α cell dysfunction in obesity and diabetes and not necessarily due to a failure of β cells as insulin levels remained comparable. Importantly, glucagon is not increased during the early phases of obesity development, which supports the notion that sympathetically released NE is the key driver of the insulin resistance that develops as early as after only 3 days. Of note, while the HFD-induced rise in NE,[19] epinephrine,[27] and glucagon[52] was completely prevented in THΔper mice, the increase in glucocorticoid levels after HFD feeding was not reduced, suggesting that obesity-induced insulin resistance can be ameliorated even though the HPA axis remains activated and/or that an increased activation of the HPA axis in the absence of a fully functional SNS is insufficient to cause obesity-induced insulin resistance.

Our work suggests that SNS-induced insulin resistance is to a large extent mediated by increased WAT lipolysis. This notion is supported by two findings, first that NE-induced insulin resistance is prevented by pharmacological inhibition of ATGL and second that AAKO mice are protected from HFD-induced insulin resistance. Our data corroborate a previous report that administration of ATGListatin prevents long-term HFD-induced insulin resistance and liver steatosis.[53] A caveat of this earlier study was that long-term treatment with ATGListatin also reduced body weight and adiposity, and hence it remained unclear if the improvement in insulin action was due to reduced adiposity or reduced lipolysis. A strength of our study is that adiposity was not a confounder. In aggregate, our studies support a model in which obesity increases the SNS, which triggers WAT lipolysis, and while increased adrenergic signaling is sufficient to induce

Figure 4. Reducing SNA improves adipose tissue dysfunction

(A and B) THΔper mice were protected from 16 weeks of HFD-induced loss of lipogenic capacity in eWAT (n = 4–11).
(C) Lipidomics analysis of plasma revealed that C16:1-palmitoleate was significantly increased in THΔper mice fed HFD (n = 3–5).
(D) Phosphorylation of HSL and perilipin was markedly suppressed after HFD feeding (n = 4–11).
(E) H&E staining of representative eWAT sections of the four subgroups (WT, THΔper, WT with HFD, THΔper with HFD). Crown-like structures (CLSs) are indicated by arrows. Scale bar, 200 μm.
(F) Weight of eWAT of THΔper mice and WT mice fed RC (n = 4–5) or HFD (n = 5–12).
(G) Adipocyte mean area, diameter, volume, and number in eWAT of THΔper mice and WT mice fed RC and HFD (n = 4–7).
(H) THΔper mice were protected from increased number of CLS induced by HFD in eWAT (n = 4–7).
(I) Pro-inflammatory gene expression in eWAT (n = 4–7).
(J) HFD-induced adipose tissue fibrosis is improved in THΔper mice as assessed by Masson's trichrome staining (n = 4–7). Scale bar, 200 μm.
(K) Senescence gene expression profile in eWAT (n = 4–7).
Data are expressed as the mean ± SEM. *p < 0.05; **p < 0.01; ***p < 0.001; ****p < 0.0001; according to a two-sided Student's t test or two-way ANOVA with Tukey's test.
See also Figure S6.

Please cite this article in press as: Sakamoto et al., Overnutrition causes insulin resistance and metabolic disorder through increased sympathetic nervous system activity, Cell Metabolism (2024), https://doi.org/10.1016/j.cmet.2024.09.012

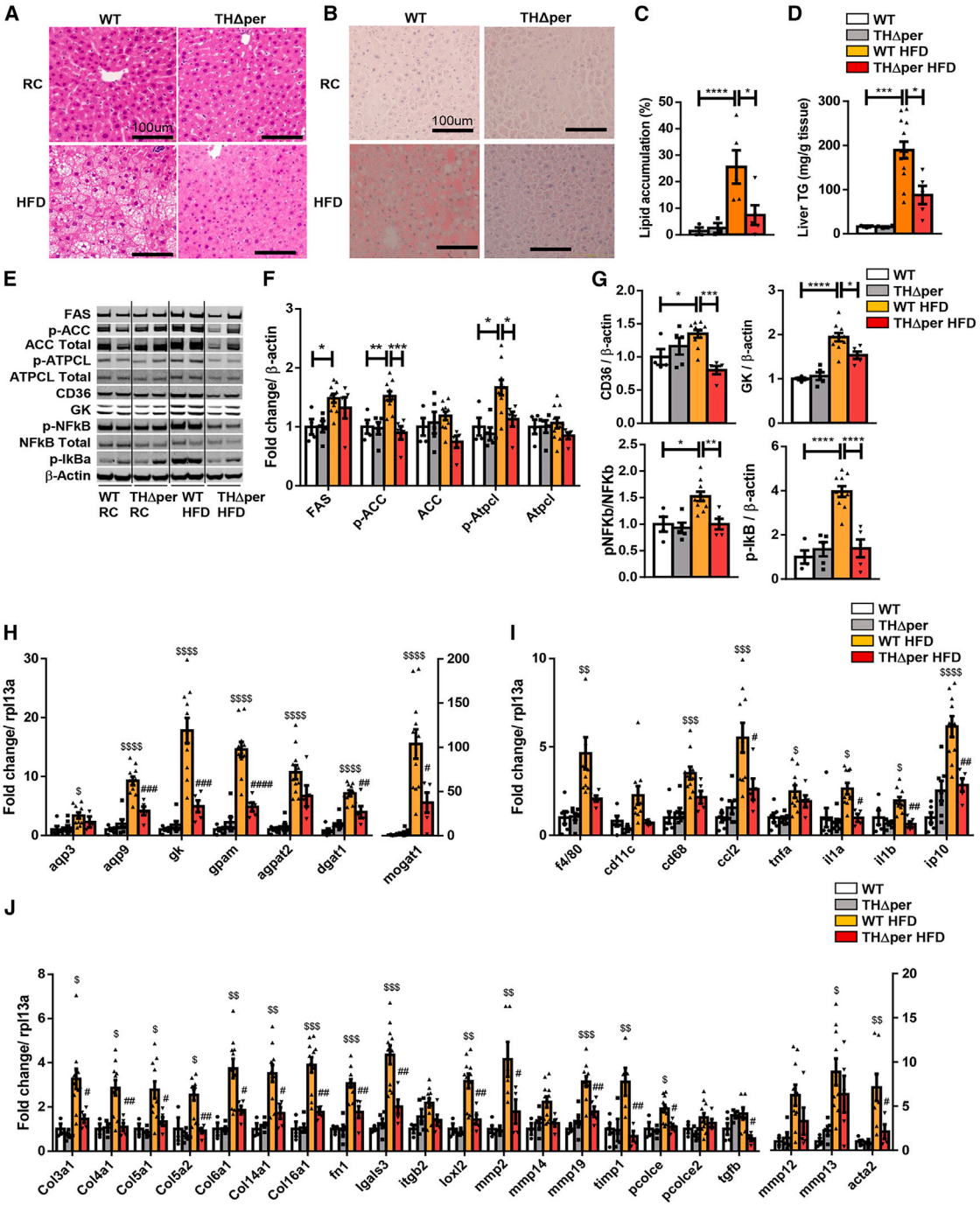

Figure 5. Reducing sympathetic stimulation ameliorates HFD feeding-induced fatty liver

(A and B) H&E staining (A) and oil red O staining (B) of representative liver sections of the four subgroups (WT, THΔper, WT with HFD, and THΔper with HFD). Scale bar, 100 μm.

(C) Percentage of hepatocytes that stained positive with oil red O (n = 3–5).

(D) 16 weeks of HFD-induced steatosis is prevented in THΔper mice as assessed by liver TG content after Folch extraction (n = 3–13).

(E and F) Hepatic DNL protein expression is reduced in THΔper mice fed HFD (n = 4–10).

(E and G) CD36 and GK protein expression is reduced in THΔper fed HFD for 16 weeks. Overnutrition-induced inflammation is prevented in THΔper mice as assessed through the activation states of NF-κB and IkB.

(H) Genes participating in TG synthesis (n = 5–11).

(legend continued on next page)

Please cite this article in press as: Sakamoto et al., Overnutrition causes insulin resistance and metabolic disorder through increased sympathetic nervous system activity, Cell Metabolism (2024), https://doi.org/10.1016/j.cmet.2024.09.012

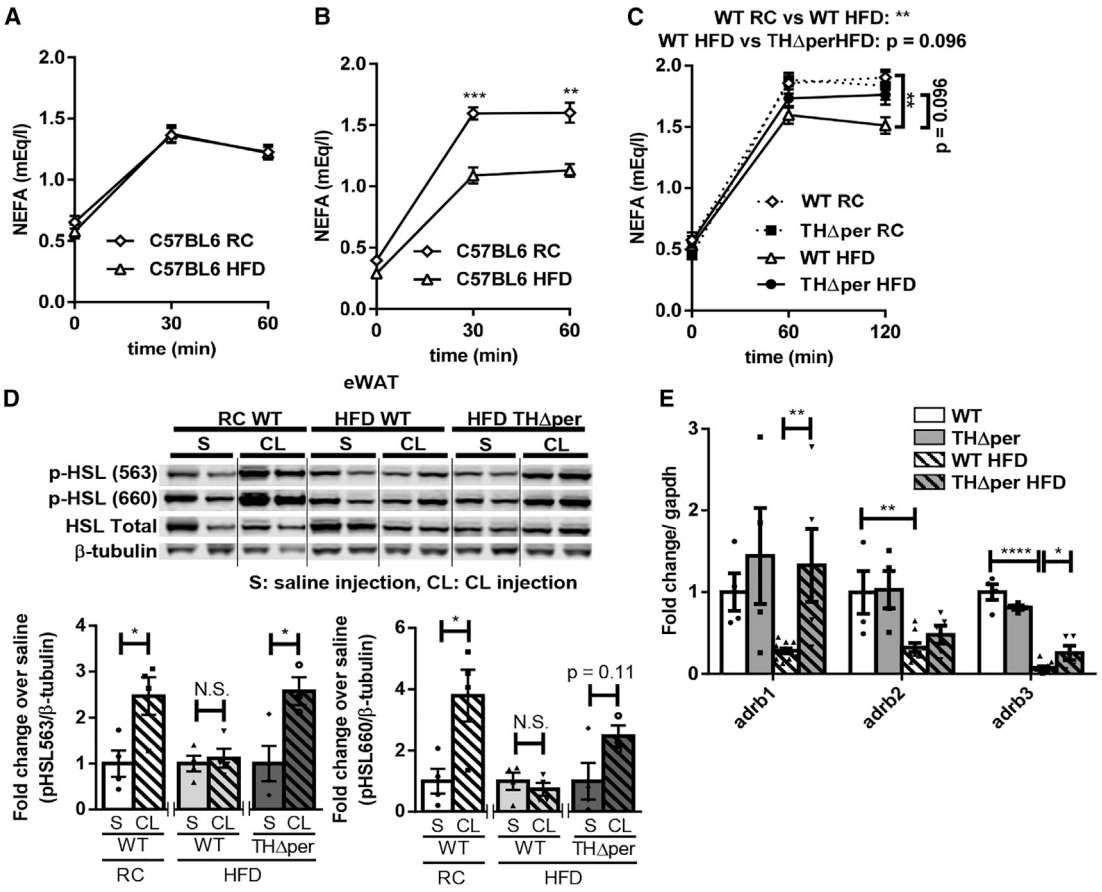

Figure 6. Reducing sympathetic activation attenuates HFD-induced CA resistance

(A and B) Plasma NEFA after CL injection in C57BL/6 mice fed RC or HFD for 3 weeks or 12 weeks (n = 5).

(C) Plasma NEFA after CL injection in THΔper mice and WT mice fed RC or HFD for 12 weeks (n = 3–10).

(D) Phosphorylation of HSL in eWAT after CL injection in THΔper mice and WT fed RC or HFD for 16 weeks (n = 3–4).

(E) Adrb gene expression in eWAT (n = 4–12).

Data are expressed as the mean ± SEM. *p < 0.05; **p < 0.01; ***p < 0.001; ****p < 0.0001; according to a two-sided Student's t test or two-way ANOVA with Tukey's test.

insulin resistance, CA- or HFD-induced insulin resistance is prevented when lipolysis is inhibited, establishing a key role of the SNS-lipolysis regulation in accounting for obesity-induced insulin resistance, which does not require impaired cellular insulin signaling.

Interestingly, a prior 4-week CL infusion study showed improved glucose tolerance, which likely is due to reduced adiposity.[54] Importantly, plasma NEFA levels were profoundly reduced in this study, consistent with the hypothesis that fatty acids and lipolysis are key drivers of insulin resistance.

The benefits of suppressing SNA are not limited to improving insulin resistance but extend to ameliorating adipose tissue dysfunction, metabolic inflammation, and MAFLD. Our data suggest that reduced lipogenic capacity in adipose tissue may serve as a surrogate marker for sympathetic overactivation in obesity and that increased SNS outflow is a key reason for reduced adipogenesis in obesity. While increased circulating fatty acids are generally associated with insulin resistance, certain fatty acids, such as palmitoleate,[40] endogenously produced through DNL and secreted from adipose tissue, seem to have favorable metabolic effects, such as improving insulin action in peripheral tissue. THΔper mice exhibited significant increase of C16:1-palmitoleate in plasma, suggesting that the reason for why palmitoleate is lower in obesity is due to elevated SNA.

Cold exposure and CL administration can increase DNL protein expression,[55] which may occur in part through the induction of insulin secretion.[56] While WAT DNL (p-Atpcl and Atpcl) tended to be lower in THΔper mice fed RC compared with WT controls, HFD feeding strongly reduced adipose tissue DNL (FAS, ACC, p-Atpcl, and Atpcl) in WT mice as described earlier,[4,5] but this

(I) Pro-inflammatory gene expression in liver (n = 3–10).

(J) Fibrosis gene expression profile in liver (n = 3–11).

Data are expressed as the mean ± SEM. *p < 0.05; **p < 0.01; ***p < 0.001; ****p < 0.0001; according to a two-sided Student's t test or two-way ANOVA with Tukey's test; (L) $ and # mean p < 0.05 vs. WT RC and WT HFD groups correspondingly.

Please cite this article in press as: Sakamoto et al., Overnutrition causes insulin resistance and metabolic disorder through increased sympathetic nervous system activity, Cell Metabolism (2024), https://doi.org/10.1016/j.cmet.2024.09.012

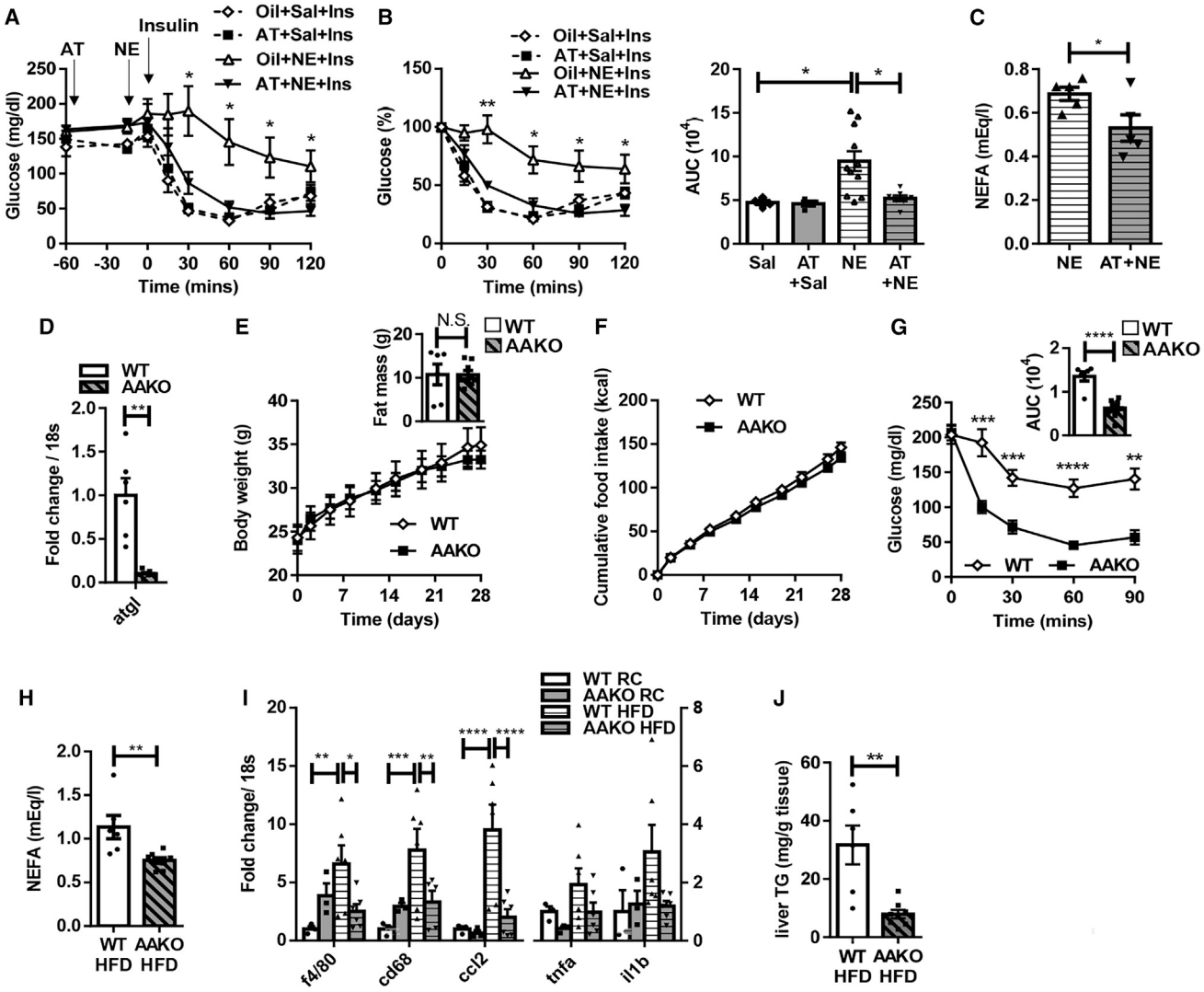

Figure 7. Adipose tissue lipolysis is a critical pathway of SNA-induced glucose intolerance

(A) Pharmacological inhibition of lipolysis through ATGListatin ameliorated NE-induced insulin resistance. ATGListatin or corn oil was administered orally by gavage 60 min before insulin injection. NE or saline were injected 15 min before insulin injection (n = 4–11).

(B) Percentage change from baseline (before insulin injection) blood glucose. Right: AUC of blood glucose.

(C) ATGListatin reduced fasting plasma NEFA levels (n = 5).

(D) Gene expression of *atgl* in eWAT (n = 6).

(E and F) Body weight (E), fat mass (E, upper right), and food intake (F) of AAKO mice and WT mice fed HFD for 28 days (n = 4–8).

(G) Plasma glucose during insulin tolerance test of AAKO mice and WT mice fed HFD for 28 days (n = 6–8). Upper right: AUC of blood glucose.

(H and J) Fasting plasma NEFA (H) and liver TG content (J) of AAKO mice and WT mice fed HFD for 28 days (n = 6–8).

(I) Pro-inflammatory gene expression in eWAT (n = 3–6).

AT, ATGListatin. Data expressed as mean ± SEM. $^{*}p < 0.05$, $^{**}p < 0.01$, $^{***}p < 0.001$, $^{****}p < 0.0001$; according to a two-sided Student's t test (A and B: * mean $p < 0.05$ vs. AT + NE + Ins) or two-way ANOVA with Tukey's test.

reduction was prevented in THΔper mice. These findings suggest that increased SNA accounts for the reduction in adipose tissue lipogenic capacity in obesity.

Our study reveals that increased SNA is an important driver of HFD-induced hepatic steatosis, the initiating event of MAFLD.[10] Reduced steatosis upon suppression of the SNS in the THΔper mice may be mediated by multiple mechanisms, including decreased fatty acid flux from WAT and lower fatty acid uptake due to reduced expression of CD36 or to decreased hepatic DNL and TG synthesis. The observation that AAKO mice on HFD are protected from hepatic TG accumulation suggests that SNA-induced unrestrained lipolysis is an important driver of hepatic steatosis in overfeeding. This evidence is consistent with reports that overexpression of β-ARs in cultured hepatocytes induces intracellular lipid accumulation,[57] suggesting an important role of β-adrenergic signaling in hepatic steatosis. NE can trigger hematopoietic stem cell (HSC) activation and proliferation, which in turn promotes liver inflammation, fibrosis,[58]

Please cite this article in press as: Sakamoto et al., Overnutrition causes insulin resistance and metabolic disorder through increased sympathetic nervous system activity, Cell Metabolism (2024), https://doi.org/10.1016/j.cmet.2024.09.012

and progression of steatohepatitis. In addition to steatosis, THΔper mice are also protected from HFD-induced liver inflammation and fibrosis, suggesting that increased SNA may contribute not only to the initiation but also to the progression of MAFLD to more advanced stages.

While more studies are needed to further characterize how SNS overdrive results in CA resistance at a tissue-specific and molecular level, our observation that CA resistance is markedly reduced in the THΔper mice provides an important insight to unravel apparently conflicting evidence of both SNS overdrive and insufficiency in obesity. Our studies suggest that SNA is indeed increased in obesity and an early driver of multiple manifestations of diet-induced metabolic disease. Prevention of obesity-induced CA resistance in the THΔper mice despite comparable adiposity gain indicates that SNS overdrive is a key reason for the CA resistance. Therefore, SNS overdrive rather than insufficiency emerges as the primary therapeutic target as mitigating SNS overactivation seems effective to improving various complications of obesity-induced metabolic disease while also ameliorating manifestations of sympathetic insufficiency and adrenergic desensitization.

In summary, this study demonstrates that overnutrition increases SNA and adipose tissue lipolysis, which emerge as pivotal drivers of obesity-induced insulin resistance as well as other hallmarks of metabolic disease such as adipose tissue dysfunction and fatty liver disease. The findings suggest a paradigm shift in our understanding of how obesity induces insulin resistance.

Limitations of the study

A limitation of our studies is that the THΔper model does not allow to assess the role of SNA overdrive in specific organs. Thus, the directionality, dynamics, and other characteristics of endogenous SNA in adipose tissue or other tissues during HFD feeding warrant further investigation. Future studies employing models of organ-specific sympathectomies will be needed to further elucidate the relative contribution of SNA in specific tissues and determine whether a global rather than tissue-specific or a peripheral vs. central targeting of SNA is more effective to ameliorate multi-organ manifestations of metabolic disease in obesity. The observation that most adrenergic blockers are not particularly beneficial in obesity suggests that a more targeted modulation of the SNS may be required to reap the benefits of reduced SNS overdrive in metabolic disease. Of note, several adrenergic blockers cross the blood-brain barrier and do not exhibit peripherally restricted action but also penetrate and act in the CNS. Further, mixed effects may be exerted when adrenergic blockers target adrenergic receptors that are already to some extent desensitized. Alternative approaches to exploit our findings for the treatment of metabolic disease in obesity may include restraining SNS outflow by enhancing brain insulin action, a potentially important upstream inhibitor of SNS outflow as we previously reported.[12,47,38] Indeed, brain insulin-sensitizing approaches such as intranasal administration of PTP1b inhibitors that have been found to improve metabolic control[59] warrant further investigation as potential avenues to modulate SNS outflow to peripheral tissues.

We studied male mice, as they are more susceptible to obesity-induced metabolic disorders. Future studies will examine the role of the SNS in females and in menopause-induced insulin resistance.

While our study revealed that acute and chronic NE infusion impaired insulin action, plasma NE reached supraphysiological levels during the NE infusion. However, it is important to note that the local concentration of NE at the sympathetic cleft that the adipocyte sees is much higher than plasma levels. Thus, to experimentally mimic NE levels at the synaptic cleft, we thought it necessary to elevate plasma NE concentrations to higher than physiological plasma levels. While we believe the results of the NE infusion study are complementary and support the hypothesis, a caveat of this study is that while the lipolytic activity of HSL in eWAT trended to be increased in the NE-infused group, NEFA levels were not different at the end of the study, likely due to increased NEFA utilization. Future studies may benefit from utilizing a mouse model that allows the direct and selective activation of the SNA to adipose tissue.

RESOURCE AVAILABILITY

Lead contact

Further information and requests for resources and reagents should be directed to the lead contact, Christoph Buettner (cb1116@rutgers.edu).

Materials availability

THΔper is available from the lead contact upon request, while the distribution is contingent upon an MTA from Taconic Biosciences.

Data and code availability

Uncropped western blots and source data can be found in Data S1. This paper does not report original code. Any additional information required to reanalyze the data reported in this paper is available from the lead contact upon request.

ACKNOWLEDGMENTS

We thank Dr. Richard Palmiter for the $TH^{flox/flox}$ mice; Dr. Henri H. Ruiz for the data regarding AAKO mice fed HFD; Dr. Xiaoyang Su and Dr. Maria Elena Diaz Rubio for lipidomics analysis; Ms. Patricia Greenberg for providing advice on statistical analysis; Dr. Susan K. Fried for advice on adipose tissue analysis; Mr. Licheng Wu and Dr. Haihong Zong for clamp study; Dr. Moshmi Bhattacharya for providing advice on liver tissue analysis; Dr. Fredric E. Wondisford and members of the Wondisford lab for helpful discussions; and Ms. Sai Siri Dasari, Mr. Nicholas Dante, Ms. Min Sun Kim, Mr. David Menna, Mr. Nader Ahmed, and Ms. Aaheli Konar for technical assistance. *Atg*Flox mice (B6N.129S-Pnpla2^{tm1Eek}/J; Stock No: 24278) were generated with Dr. Erin E. Kershaw with grant support from NIH R01 DK090166. The graphical abstract was created with biorender.com. This study was supported by the following grants: DK074873, DK083568, and DK082724 (C.B.); the Department of Defense (W81XWH-22-1-0200) and the Manpei Suzuki Diabetes Foundation (K.S.); and the National Institutes of Health (R01 HL162773), the Department of Veterans Affairs (BX004249 and BX006040), and the University of Iowa Fraternal Order of Eagles Diabetes Research Center (K.R.).

AUTHOR CONTRIBUTIONS

K.S. obtained funding, designed research, performed experiments, analyzed data, and wrote the paper. M.A.B., C.Z., and G.M. contributed to the studies. B.C., L.L., A.S., L.P., K.T., V.C., and A.T. assisted with experiments. G.J.S. supervised clamps in Figure 3 and edited the paper. K.R. and D.A.M. performed nerve recording in Figure 2. C.B. conceived the studies, obtained funding, designed the research, wrote the paper, and supervised the project.

DECLARATION OF INTERESTS

C.B. received research support from Pfizer and consulted for Boehringer and Novo Nordisk, all of which were unrelated to the work described in this manuscript. G.M. is part of the editorial team at Elsevier.

STAR★METHODS

Detailed methods are provided in the online version of this paper and include the following:

- KEY RESOURCES TABLE
- EXPERIMENTAL MODEL AND SUBJECT DETAILS
  - Mice
  - Body weight and Food Intake
  - Body composition
  - Glucose Tolerance Test
  - Insulin Tolerance Test
  - Cold tolerance test
  - Hyperinsulinemic-Euglycemic Clamps
  - Acute NE infusion
  - Chronic NE infusion
  - Insulin signaling
  - 2-DG Treatment
  - ATGListatin and NE treatment before Insulin tolerance test
  - CL 316,243 treatment
- METHOD DETAILS
  - Western blot
  - Preparation of RNA and gene-expression analysis
  - Hepatic TG Extraction
  - Histology
  - Plasma Assays
  - Lipidomics analysis
  - BAT thermal imaging
  - Inguinal and Gonadal SNA Recording
- QUANTIFICATION AND STATISTICAL ANALYSIS
  - Statistics

SUPPLEMENTAL INFORMATION

Supplemental information can be found online at https://doi.org/10.1016/j.cmet.2024.09.012.

Received: January 9, 2024
Revised: June 19, 2024
Accepted: September 23, 2024
Published: October 21, 2024

REFERENCE

1. Must, A., Spadano, J., Coakley, E.H., Field, A.E., Colditz, G., and Dietz, W.H. (1999). The disease burden associated with overweight and obesity. JAMA *282*, 1523–1529. https://doi.org/10.1001/jama.282.16.1523.
2. Choe, S.S., Huh, J.Y., Hwang, I.J., Kim, J.I., and Kim, J.B. (2016). Adipose tissue remodeling: its role in energy metabolism and metabolic disorders. Front. Endocrinol. (Lausanne) *7*, 30. https://doi.org/10.3389/fendo.2016.00030.
3. Boden, G. (2006). Fatty acid-induced inflammation and insulin resistance in skeletal muscle and liver. Curr. Diab. Rep. *6*, 177–181. https://doi.org/10.1007/s11892-006-0031-x.
4. Eissing, L., Scherer, T., Tödter, K., Knippschild, U., Greve, J.W., Buurman, W.A., Pinnschmidt, H.O., Rensen, S.S., Wolf, A.M., Bartelt, A., et al. (2013). De novo lipogenesis in human fat and liver is linked to ChREBP-beta and metabolic health. Nat. Commun. *4*, 1528. https://doi.org/10.1038/ncomms2537.
5. Song, Z., Xiaoli, A.M., and Yang, F. (2018). Regulation and metabolic significance of de novo lipogenesis in adipose tissues. Nutrients *10*, 1383. https://doi.org/10.3390/nu10101383.
6. Zatterale, F., Longo, M., Naderi, J., Raciti, G.A., Desiderio, A., Miele, C., and Beguinot, F. (2019). Chronic adipose tissue inflammation linking obesity to insulin resistance and type 2 diabetes. Front. Physiol. *10*, 1607. https://doi.org/10.3389/fphys.2019.01607.
7. Crewe, C., An, Y.A., and Scherer, P.E. (2017). The ominous triad of adipose tissue dysfunction: inflammation, fibrosis, and impaired angiogenesis. J. Clin. Invest. *127*, 74–82. https://doi.org/10.1172/JCI88883.
8. Magnusson, I., Rothman, D.L., Katz, L.D., Shulman, R.G., and Shulman, G.I. (1992). Increased rate of gluconeogenesis in type II diabetes mellitus. A 13C nuclear magnetic resonance study. J. Clin. Invest. *90*, 1323–1327. https://doi.org/10.1172/JCI115997.
9. Tilg, H., Moschen, A.R., and Roden, M. (2017). NAFLD and diabetes mellitus. Nat. Rev. Gastroenterol. Hepatol. *14*, 32–42. https://doi.org/10.1038/nrgastro.2016.147.
10. Eslam, M., El-Serag, H.B., Francque, S., Sarin, S.K., Wei, L., Bugianesi, E., and George, J. (2022). Metabolic (dysfunction)-associated fatty liver disease in individuals of normal weight. Nat. Rev. Gastroenterol. Hepatol. *19*, 638–651. https://doi.org/10.1038/s41575-022-00635-5.
11. Boucher, J., Kleinridders, A., and Kahn, C.R. (2014). Insulin receptor signaling in normal and insulin-resistant states. Cold Spring Harb. Perspect. Biol. *6*, a009191. https://doi.org/10.1101/cshperspect.a009191.
12. Scherer, T., Lindtner, C., Zielinski, E., O'Hare, J., Filatova, N., and Buettner, C. (2012). Short term voluntary overfeeding disrupts brain insulin control of adipose tissue lipolysis. J. Biol. Chem. *287*, 33061–33069. https://doi.org/10.1074/jbc.M111.307348.
13. O'Hare, J.D., Zielinski, E., Cheng, B., Scherer, T., and Buettner, C. (2011). Central endocannabinoid signaling regulates hepatic glucose production and systemic lipolysis. Diabetes *60*, 1055–1062. https://doi.org/10.2337/db10-0962.
14. Jones, P.P., Davy, K.P., Alexander, S., and Seals, D.R. (1997). Age-related increase in muscle sympathetic nerve activity is associated with abdominal adiposity. Am. J. Physiol. *272*, E976–E980. https://doi.org/10.1152/ajpendo.1997.272.6.E976.
15. Grassi, G., Dell'Oro, R., Quarti-Trevano, F., Scopelliti, F., Seravalle, G., Paleari, F., Gamba, P.L., and Mancia, G. (2005). Neuroadrenergic and reflex abnormalities in patients with metabolic syndrome. Diabetologia *48*, 1359–1365. https://doi.org/10.1007/s00125-005-1798-z.
16. Wang, P., Loh, K.H., Wu, M., Morgan, D.A., Schneeberger, M., Yu, X., Chi, J., Kosse, C., Kim, D., Rahmouni, K., et al. (2020). A leptin-BDNF pathway regulating sympathetic innervation of adipose tissue. Nature *583*, 839–844. https://doi.org/10.1038/s41586-020-2527-y.
17. Liu, K., Yang, L., Wang, G., Liu, J., Zhao, X., Wang, Y., Li, J., and Yang, J. (2021). Metabolic stress drives sympathetic neuropathy within the liver. Cell Metab. *33*, 666–675.e4. https://doi.org/10.1016/j.cmet.2021.01.012.
18. Hurr, C., Simonyan, H., Morgan, D.A., Rahmouni, K., and Young, C.N. (2019). Liver sympathetic denervation reverses obesity-induced hepatic steatosis. J. Physiol. *597*, 4565–4580. https://doi.org/10.1113/JP277994.
19. Nguyen, L.V., Ta, Q.V., Dang, T.B., Nguyen, P.H., Nguyen, T., Pham, T.V.H., Nguyen, T.H., Baker, S., Le Tran, T., Yang, D.J., et al. (2019). Carvedilol improves glucose tolerance and insulin sensitivity in treatment of adrenergic overdrive in high fat diet-induced obesity in mice. PLoS One *14*, e0224674. https://doi.org/10.1371/journal.pone.0224674.
20. Mowers, J., Uhm, M., Reilly, S.M., Simon, J., Leto, D., Chiang, S.H., Chang, L., and Saltiel, A.R. (2013). Inflammation produces catecholamine resistance in obesity via activation of PDE3B by the protein kinases IKKepsilon and TBK1. eLife *2*, e01119. https://doi.org/10.7554/eLife.01119.
21. Reilly, S.M., and Saltiel, A.R. (2017). Adapting to obesity with adipose tissue inflammation. Nat. Rev. Endocrinol. *13*, 633–643. https://doi.org/10.1038/nrendo.2017.90.

22. Arner, P. (1999). Catecholamine-induced lipolysis in obesity. Int. J. Obes. Relat. Metab. Disord. *23* (*Suppl 1*), 10–13. https://doi.org/10.1038/sj.ijo.0800789.

23. Valentine, J.M., Ahmadian, M., Keinan, O., Abu-Odeh, M., Zhao, P., Zhou, X., Keller, M.P., Gao, H., Yu, R.T., Liddle, C., et al. (2022). β3-Adrenergic receptor downregulation leads to adipocyte catecholamine resistance in obesity. J. Clin. Invest. *132*, e153357. https://doi.org/10.1172/JCI153357.

24. Okeke, K., Angers, S., Bouvier, M., and Michel, M.C. (2019). Agonist-induced desensitisation of β_3 -adrenoceptors: Where, when, and how? Br. J. Pharmacol. *176*, 2539–2558. https://doi.org/10.1111/bph.14633.

25. Baron, A.D., Schaeffer, L., Shragg, P., and Kolterman, O.G. (1987). Role of hyperglucagonemia in maintenance of increased rates of hepatic glucose output in type II diabetics. Diabetes *36*, 274–283. https://doi.org/10.2337/diab.36.3.274.

26. Lager, I. (1991). The insulin-antagonistic effect of the counterregulatory hormones. J. Intern. Med. Suppl. *735*, 41–47.

27. Cristino, L., Busetto, G., Imperatore, R., Ferrandino, I., Palomba, L., Silvestri, C., Petrosino, S., Orlando, P., Bentivoglio, M., Mackie, K., et al. (2013). Obesity-driven synaptic remodeling affects endocannabinoid control of orexinergic neurons. Proc. Natl. Acad. Sci. USA *110*, E2229–E2238. https://doi.org/10.1073/pnas.1219485110.

28. Eikelis, N., Lambert, G., Wiesner, G., Kaye, D., Schlaich, M., Morris, M., Hastings, J., Socratous, F., and Esler, M. (2004). Extra-adipocyte leptin release in human obesity and its relation to sympathoadrenal function. Am. J. Physiol. Endocrinol. Metab. *286*, E744–E752. https://doi.org/10.1152/ajpendo.00489.2003.

29. Reaven, G.M., Chen, Y.D., Golay, A., Swislocki, A.L., and Jaspan, J.B. (1987). Documentation of hyperglucagonemia throughout the day in nonobese and obese patients with noninsulin-dependent diabetes mellitus. J. Clin. Endocrinol. Metab. *64*, 106–110. https://doi.org/10.1210/jcem-64-1-106.

30. Cooperberg, B.A., and Cryer, P.E. (2010). Insulin reciprocally regulates glucagon secretion in humans. Diabetes *59*, 2936–2940. https://doi.org/10.2337/db10-0728.

31. Lee, Y.S., Li, P., Huh, J.Y., Hwang, I.J., Lu, M., Kim, J.I., Ham, M., Talukdar, S., Chen, A., Lu, W.J., et al. (2011). Inflammation is necessary for long-term but not short-term high-fat diet-induced insulin resistance. Diabetes *60*, 2474–2483. https://doi.org/10.2337/db11-0194.

32. Czech, M.P. (2017). Insulin action and resistance in obesity and type 2 diabetes. Nat. Med. *23*, 804–814. https://doi.org/10.1038/nm.4350.

33. Buettner, C., Muse, E.D., Cheng, A., Chen, L., Scherer, T., Pocai, A., Su, K., Cheng, B., Li, X., Harvey-White, J., et al. (2008). Leptin controls adipose tissue lipogenesis via central, STAT3-independent mechanisms. Nat. Med. *14*, 667–675. https://doi.org/10.1038/nm1775.

34. Brito, M.N., Brito, N.A., Baro, D.J., Song, C.K., and Bartness, T.J. (2007). Differential activation of the sympathetic innervation of adipose tissues by melanocortin receptor stimulation. Endocrinology *148*, 5339–5347. https://doi.org/10.1210/en.2007-0621.

35. Fischer, K., Ruiz, H.H., Jhun, K., Finan, B., Oberlin, D.J., van der Heide, V., Kalinovich, A.V., Petrovic, N., Wolf, Y., Clemmensen, C., et al. (2017). Alternatively activated macrophages do not synthesize catecholamines or contribute to adipose tissue adaptive thermogenesis. Nat. Med. *23*, 623–630. https://doi.org/10.1038/nm.4316.

36. Madden, C.J., and Morrison, S.F. (2016). A high-fat diet impairs cooling-evoked brown adipose tissue activation via a vagal afferent mechanism. Am. J. Physiol. Endocrinol. Metab. *311*, E287–E292. https://doi.org/10.1152/ajpendo.00081.2016.

37. Bartness, T.J., Shrestha, Y.B., Vaughan, C.H., Schwartz, G.J., and Song, C.K. (2010). Sensory and sympathetic nervous system control of white adipose tissue lipolysis. Mol. Cell. Endocrinol. *318*, 34–43. https://doi.org/10.1016/j.mce.2009.08.031.

38. Scherer, T., Sakamoto, K., and Buettner, C. (2021). Brain insulin signalling in metabolic homeostasis and disease. Nat. Rev. Endocrinol. *17*, 468–483. https://doi.org/10.1038/s41574-021-00498-x.

39. Ou, M.Y., Zhang, H., Tan, P.C., Zhou, S.B., and Li, Q.F. (2022). Adipose tissue aging: mechanisms and therapeutic implications. Cell Death Dis. *13*, 300. https://doi.org/10.1038/s41419-022-04752-6.

40. Cao, H., Gerhold, K., Mayers, J.R., Wiest, M.M., Watkins, S.M., and Hotamisligil, G.S. (2008). Identification of a lipokine, a lipid hormone linking adipose tissue to systemic metabolism. Cell *134*, 933–944. https://doi.org/10.1016/j.cell.2008.07.048.

41. Primeau, V., Coderre, L., Karelis, A.D., Brochu, M., Lavoie, M.E., Messier, V., Sladek, R., and Rabasa-Lhoret, R. (2011). Characterizing the profile of obese patients who are metabolically healthy. Int. J. Obes. (Lond) *35*, 971–981. https://doi.org/10.1038/ijo.2010.216.

42. Kusminski, C.M., Holland, W.L., Sun, K., Park, J., Spurgin, S.B., Lin, Y., Askew, G.R., Simcox, J.A., McClain, D.A., Li, C., et al. (2012). MitoNEET-driven alterations in adipocyte mitochondrial activity reveal a crucial adaptive process that preserves insulin sensitivity in obesity. Nat. Med. *18*, 1539–1549. https://doi.org/10.1038/nm.2899.

43. Suda, M., Shimizu, I., Katsuumi, G., Yoshida, Y., Hayashi, Y., Ikegami, R., Matsumoto, N., Yoshida, Y., Mikawa, R., Katayama, A., et al. (2021). Senolytic vaccination improves normal and pathological age-related phenotypes and increases lifespan in progeroid mice. Nat. Aging *1*, 1117–1126. https://doi.org/10.1038/s43587-021-00151-2.

44. Koonen, D.P.Y., Jacobs, R.L., Febbraio, M., Young, M.E., Soltys, C.L.M., Ong, H., Vance, D.E., and Dyck, J.R.B. (2007). Increased hepatic CD36 expression contributes to dyslipidemia associated with diet-induced obesity. Diabetes *56*, 2863–2871. https://doi.org/10.2337/db07-0907.

45. Reshef, L., Olswang, Y., Cassuto, H., Blum, B., Croniger, C.M., Kalhan, S.C., Tilghman, S.M., and Hanson, R.W. (2003). Glyceroneogenesis and the triglyceride/fatty acid cycle. J. Biol. Chem. *278*, 30413–30416. https://doi.org/10.1074/jbc.R300017200.

46. Lowell, B.B., and Bachman, E.S. (2003). Beta-Adrenergic receptors, diet-induced thermogenesis, and obesity. J. Biol. Chem. *278*, 29385–29388. https://doi.org/10.1074/jbc.R300011200.

47. Scherer, T., O'Hare, J., Diggs-Andrews, K., Schweiger, M., Cheng, B., Lindtner, C., Zielinski, E., Vempati, P., Su, K., Dighe, S., et al. (2011). Brain insulin controls adipose tissue lipolysis and lipogenesis. Cell Metab. *13*, 183–194. https://doi.org/10.1016/j.cmet.2011.01.008.

48. Mayer, N., Schweiger, M., Romauch, M., Grabner, G.F., Eichmann, T.O., Fuchs, E., Ivkovic, J., Heier, C., Mrak, I., Lass, A., et al. (2013). Development of small-molecule inhibitors targeting adipose triglyceride lipase. Nat. Chem. Biol. *9*, 785–787. https://doi.org/10.1038/nchembio.1359.

49. Schoiswohl, G., Stefanovic-Racic, M., Menke, M.N., Wills, R.C., Surlow, B.A., Basantani, M.K., Sitnick, M.T., Cai, L., Yazbeck, C.F., Stolz, D.B., et al. (2015). Impact of reduced ATGL-mediated adipocyte lipolysis on obesity-associated insulin resistance and inflammation in male mice. Endocrinology *156*, 3610–3624. https://doi.org/10.1210/en.2015-1322.

50. Lyu, K., Zhang, D., Song, J., Li, X., Perry, R.J., Samuel, V.T., and Shulman, G.I. (2021). Short-term overnutrition induces white adipose tissue insulin resistance through sn-1,2-diacylglycerol/PKCepsilon/insulin receptor Thr1160 phosphorylation. JCI Insight *6*, e139946. https://doi.org/10.1172/jci.insight.139946.

51. Turner, N., Kowalski, G.M., Leslie, S.J., Risis, S., Yang, C., Lee-Young, R.S., Babb, J.R., Meikle, P.J., Lancaster, G.I., Henstridge, D.C., et al. (2013). Distinct patterns of tissue-specific lipid accumulation during the induction of insulin resistance in mice by high-fat feeding. Diabetologia *56*, 1638–1648. https://doi.org/10.1007/s00125-013-2913-1.

52. Kellard, J.A., Rorsman, N.J.G., Hill, T.G., Armour, S.L., van de Bunt, M., Rorsman, P., Knudsen, J.G., and Briant, L.J.B. (2020). Reduced somatostatin signalling leads to hypersecretion of glucagon in mice fed a high-fat diet. Mol. Metab. *40*, 101021. https://doi.org/10.1016/j.molmet.2020.101021.

53. Schweiger, M., Romauch, M., Schreiber, R., Grabner, G.F., Hütter, S., Kotzbeck, P., Benedikt, P., Eichmann, T.O., Yamada, S., Knittelfelder, O., et al. (2017). Pharmacological inhibition of adipose triglyceride lipase

corrects high-fat diet-induced insulin resistance and hepatosteatosis in mice. Nat. Commun. *8*, 14859. https://doi.org/10.1038/ncomms14859.

54. Xiao, C., Goldgof, M., Gavrilova, O., and Reitman, M.L. (2015). Anti-obesity and metabolic efficacy of the β3-adrenergic agonist, CL316243, in mice at thermoneutrality compared to 22°C. Obesity (Silver Spring) *23*, 1450–1459. https://doi.org/10.1002/oby.21124.
55. Guilherme, A., Yenilmez, B., Bedard, A.H., Henriques, F., Liu, D., Lee, A., Goldstein, L., Kelly, M., Nicoloro, S.M., Chen, M., et al. (2020). Control of adipocyte thermogenesis and lipogenesis through β3-adrenergic and thyroid hormone signal integration. Cell Rep. *31*, 107598. https://doi.org/10.1016/j.celrep.2020.107598.
56. Heine, M., Fischer, A.W., Schlein, C., Jung, C., Straub, L.G., Gottschling, K., Mangels, N., Yuan, Y., Nilsson, S.K., Liebscher, G., et al. (2018). Lipolysis triggers a systemic insulin response essential for efficient energy replenishment of activated brown adipose tissue in mice. Cell Metab. *28*, 644–655.e4. https://doi.org/10.1016/j.cmet.2018.06.020.
57. Ghosh, P.M., Shu, Z.J., Zhu, B., Lu, Z., Ikeno, Y., Barnes, J.L., Yeh, C.K., Zhang, B.X., Katz, M.S., and Kamat, A. (2012). Role of beta-adrenergic receptors in regulation of hepatic fat accumulation during aging. J. Endocrinol. *213*, 251–261. https://doi.org/10.1530/JOE-11-0406.
58. Oben, J.A., Yang, S., Lin, H., Ono, M., and Diehl, A.M. (2003). Norepinephrine and neuropeptide Y promote proliferation and collagen gene expression of hepatic myofibroblastic stellate cells. Biochem. Biophys. Res. Commun. *302*, 685–690. https://doi.org/10.1016/s0006-291x(03)00232-8.
59. Dodd, G.T., Xirouchaki, C.E., Eramo, M., Mitchell, C.A., Andrews, Z.B., Henry, B.A., Cowley, M.A., and Tiganis, T. (2019). Intranasal targeting of hypothalamic PTP1B and TCPTP reinstates leptin and insulin sensitivity and promotes weight loss in obesity. Cell Rep. *28*, 2905–2922.e5. https://doi.org/10.1016/j.celrep.2019.08.019.
60. Koch, L., Wunderlich, F.T., Seibler, J., Könner, A.C., Hampel, B., Irlenbusch, S., Brabant, G., Kahn, C.R., Schwenk, F., and Brüning, J.C. (2008). Central insulin action regulates peripheral glucose and fat metabolism in mice. J. Clin. Invest. *118*, 2132–2147. https://doi.org/10.1172/JCI31073.
61. Sitnick, M.T., Basantani, M.K., Cai, L., Schoiswohl, G., Yazbeck, C.F., Distefano, G., Ritov, V., DeLany, J.P., Schreiber, R., Stolz, D.B., et al. (2013). Skeletal muscle triacylglycerol hydrolysis does not influence metabolic complications of obesity. Diabetes *62*, 3350–3361. https://doi.org/10.2337/db13-0500.
62. Shin, A.C., Filatova, N., Lindtner, C., Chi, T., Degann, S., Oberlin, D., and Buettner, C. (2017). Insulin receptor signaling in POMC, but not AgRP, neurons controls adipose tissue insulin action. Diabetes *66*, 1560–1571. https://doi.org/10.2337/db16-1238.
63. Lindtner, C., Scherer, T., Zielinski, E., Filatova, N., Fasshauer, M., Tonks, N.K., Puchowicz, M., and Buettner, C. (2013). Binge drinking induces whole-body insulin resistance by impairing hypothalamic insulin action. Sci. Transl. Med. *5*, 170ra14. https://doi.org/10.1126/scitranslmed.3005123.
64. Folch, J., Lees, M., and Sloane Stanley, G.H. (1957). A simple method for the isolation and purification of total lipides from animal tissues. J. Biol. Chem. *226*, 497–509. https://doi.org/10.1016/S0021-9258(18)64849-5.
65. Wu, Y., Lee, M.J., Ido, Y., and Fried, S.K. (2017). High-fat diet-induced obesity regulates MMP3 to modulate depot- and sex-dependent adipose expansion in C57BL/6J mice. Am. J. Physiol. Endocrinol. Metab. *312*, E58–E71. https://doi.org/10.1152/ajpendo.00128.2016.
66. Crane, J.D., Mottillo, E.P., Farncombe, T.H., Morrison, K.M., and Steinberg, G.R. (2014). A standardized infrared imaging technique that specifically detects UCP1-mediated thermogenesis in vivo. Mol. Metab. *3*, 490–494. https://doi.org/10.1016/j.molmet.2014.04.007.
67. Kordić, M., Dugandžić, J., Ratko, M., Habek, N., and Dugandžić, A. (2022). Infrared thermography for the detection of changes in brown adipose tissue activity. J. Vis. Exp. e64463. https://doi.org/10.3791/64463.

Please cite this article in press as: Sakamoto et al., Overnutrition causes insulin resistance and metabolic disorder through increased sympathetic nervous system activity, Cell Metabolism (2024), https://doi.org/10.1016/j.cmet.2024.09.012

STAR★METHODS

KEY RESOURCES TABLE

REAGENT or RESOURCE	SOURCE	IDENTIFIER
Antibodies		
p-Akt (Ser473)	Cell Signaling	9271; RRID: AB_329825
p-Akt (Thr 308)	Cell Signaling	2965; RRID: AB_2255933
Akt	Cell Signaling	9272; RRID: AB_329827
p-INSR (Tyr1162)	Cell Signaling	3918; RRID: AB_10548764
INSR MA-20	Santa Cruz	sc-57344; RRID: AB_782041
p-GSK3β (pSer9)	Cell Signaling	5558; RRID: AB_10013750
GSK3β	Cell Signaling	12456; RRID: AB_2636978
p-PDE3B	FabGennix International Incorporated	PPD3B-140AP
Fatty acid synthase (FAS)	BD Biosciences	610962; RRID: AB_398275
Acetyl-CoA carboxylase (ACC)	Cell Signaling	3662; RRID: AB_2219400
Phospho-ACC(Ser79)	Cell Signaling	3661; RRID: AB_330337
ATP-Citrate Lyase (ATPCL)	Cell Signaling	4332; RRID: AB_2223744
Phospho-ATPCL	Cell Signaling	4331; RRID: AB_2257987
Glycerol kinase	Abcam	ab126599; RRID: AB_11129767
CD36	Abcam	ab133625; RRID: AB_2716564
β-actin	Santa Cruz	sc-81178; RRID: AB_2223230
Perilipin 1	Cell Signaling	9349; RRID: AB_10829911
Phospho-PKA substrate (p-perilipin)	Cell Signaling	9624; RRID: AB_331817
TH	Millipore Sigma	MAB318; RRID: AB_2201528
Cre Recombinase	Cell Signaling	15036; RRID: AB_2798694
ATGL	Cell Signaling	2138; RRID: AB_2167955
HSL	Cell Signaling	4107; RRID: AB_2296900
p-HSL (S563)	Cell Signaling	4139; RRID: AB_2135495
p-HSL (S660)	Cell Signaling	4126; RRID: AB_490997
NFκBp65	Cell Signaling	8242; RRID: AB_10859369
p-P65	Cell Signaling	3033; RRID: AB_331284
p-IκBα (Ser32)	Cell Signaling	2859; RRID: AB_561111
IκBα	Cell Signaling	4814; RRID: AB_390781
IRDye 680RD Donkey anti-Mouse IgG Secondary Antibody	LI-COR	926-68072; RRID: AB_10953628
IRDye 800CW Donkey anti-Rabbit IgG Secondary Antibody	LI-COR	926-32213; RRID: AB_621848
Chemicals, peptides, and recombinant proteins		
Odyssey LI-COR Blocking Buffer	LI-COR	927-40000
NuPAGE 4 to 12% Gel	Thermo Fisher	WG1403A
QIAzol Lysis Reagent	Qiagen	79306
RNeasy Mini Kit	Qiagen	74104
SuperScript III First-Strand Synthesis SuperMix	Thermo Fisher	11752050
SYBR green	Thermo Fisher	4309155
Glucose	Sigma	D9434
Tamoxifen	Sigma-Aldrich	T5648
CL-316,243	Sigma-Aldrich	C5976
2-Deoxy-D-glucose (2-DG)	Sigma-Aldrich	D6134
DL-Norepinephrine hydrochloride	Sigma-Aldrich	A7256

(*Continued on next page*)

Please cite this article in press as: Sakamoto et al., Overnutrition causes insulin resistance and metabolic disorder through increased sympathetic nervous system activity, Cell Metabolism (2024), https://doi.org/10.1016/j.cmet.2024.09.012

Continued

REAGENT or RESOURCE	SOURCE	IDENTIFIER
ATGListatin	Selleckchem	S7364
HR Series NEFA-HR(2) Color Reagent A	Wako	999-34691
HR series NEFA-HR(2) solvent A	Wako	995-34791
HR Series NEFA-HR(2) Color Reagent B	Wako	991-34891
HR series NEFA-HR(2) solvent B	Wako	993-35191
NEFA standard solution	Wako	276-76491
Critical commercial assays		
BCA protein assay kit	Thermo Fisher	23225
Serum triglyceride determination kit	Sigma	TR0100
Triglyceride assay kit	Thermo Fisher	TR22421
Noradrenaline (Norepinephrine) High Sensitive ELISA	Eagle Biosciences	NOU39-K01
Adrenaline (Epinephrine) High Sensitive ELISA	Eagle Biosciences	ADU39-K01
Ultrasensitive Mouse Insulin ELISA	Mercodia	10-1249-01
Glucagon ELISA	Mercodia	10-1281-01
Corticosterone Parameter Assay Kit	R&D Systems	KGE009
Experimental models: Organisms/strains		
$TH^{flox/flox}$ mice	Dr. R. Palmiter (University of Washington)	N/A
$Rosa26^{CreERT2\ mice}$	Taconic	model 10471
$ATGL^{flox/flox}$ (B6N.129-$Pnpla2^{tm1Eek}$/J) mice	Dr. Erin E. Kershaw; Jackson Laboratory	Strain 024278
B6N.FVB.Tg (Adipoq-Cre)1evr/J mice	Jackson Laboratory	Strain 028020
C57BL/6J mice	Jackson Laboratory	Strain 000664
Oligonucleotides		
Primers for genotyping, see Table S1	This paper	N/A
Primers for qPCR, see Table S1	This paper	N/A
Software and algorithms		
GraphPad Prism 8 software	GraphPad	N/A
Bioquant Life Science	Bioquant Image Analysis	N/A
Image J	Schneider et al.	https://imagej.nih.gov/ij/
Image Studio 5.2	LICOR	N/A
Other		
SpectraMax i3x Multi-Mode Microplate Reader	Molecular Devices	i3x
QuantStudio 6 Flex Real-Time PCR Systems	Thermo Fisher	4485691
Tissue-Tek O.C.T. Compound	VWR	25608-930
Olympus microscope	Olympus	BX53
LI-COR Odyssey	LI-COR	Odyssey 9140 CLx
Infrared camera, T530, emissivity of 0.95, FLIR Systems	Teledyne FLIR	N/A

EXPERIMENTAL MODEL AND SUBJECT DETAILS

Mice

Mice were fed ad libitum either a standard rodent chow diet (RC, PicoLab Rodent Diet 20-5053; LabDiet, St. Louis, MO, USA) or a HFD with 60% kcal fat (D12492i; Research Diets, New Brunswick,NJ, USA), or a HFD with 58% kcal fat (D12331; Research Diets, New Brunswick, NJ). In all studies we used D12492i, except for the nerve recording studies performed in the Rahmouni Lab (Figure 2N) in which diet D12331 was used. Animals were housed on a 12 h light/12 h dark cycle with lights on at 07:00 and off at 19:00. The ambient temperature was maintained at 21±1 °C. Only male mice were used in this study. We generated inducible peripheral *th* knockout mice by crossing $TH^{flox/flox}$ mice (kindly provided by Dr. Richard Palmiter, University of Washington) with tamoxifen-inducible $Rosa26^{CreERT2}$ mice (Taconic #10471, Hudson, NY). $TH^{flox/flox}$, $Rosa26^{CreERT2+/-}$ mice (THΔper) and the $TH^{flox/flox}$, $Rosa26^{CreERT2-/-}$ (WT littermates) expressed normal levels of TH protein during development and before induction of KO. Deletion

of the *th* gene was achieved by intraperitoneal (i.p.) injection of 50 mg/kg tamoxifen (Cat#: T5648; Sigma-Aldrich) daily for five doses administration and was limited to the periphery, owing to low expression of Cre recombinase in the CNS.[60] THΔper and WT littermates were both injected with tamoxifen at the age of 8 weeks.

We generated adipose-specific ATGLKO mice by crossing B6N.129-Pnpla2^{tm1Eek}/J[61] (ATGL$^{flox/flox}$, kindly provided by Dr. Erin E. Kershaw) with B6N.FVB.Tg (Adipoq-Cre)1evr/J mice (stock No. 028020, Jackson Laboratory, Bar Harbor ME) for at least 10 generations. The offspring either lacked ATGL in adipose (ATGL$^{flox/flox}$, Adipoq-Cre+/- or AAKO) or were the floxed, cre negative wild type littermate controls (ATGL$^{flox/flox}$, Adipoq-Cre-/- or WT).

All animal studies were carried out in accordance with protocols approved by the Institutional Animal Care and Use Committee (IACUC) in Rutgers Robert Wood Johnson Medical School, Icahn School of Medicine at Mount Sinai, and University of Iowa.

Body weight and Food Intake

Eight-week-old male WT and THΔper mice were injected with tamoxifen, then fed either HFD or RC, and body weight was measured for 10 weeks. Food remaining in the hopper of individually housed mice was measured once a week during the 10 weeks.

Body composition

We analyzed body composition (fat and lean mass) using a magnetic-resonance whole-body composition analyzer (Echo MRI, Houston, TX).

Glucose Tolerance Test

Mice were fasted for 5 hours before i.p. administration of glucose (2 g/kg body weight) dissolved in normal saline. Blood glucose level was measured with a strip-based glucometer at 0, 15, 30, 60, 90 and 120 min after the glucose injection (Contour next, Ascensia Diabetes Care US, Parsippany, NJ).

In Figure 1F, the fasting glucose level after 3 days of HFD feeding is derived from the baseline glucose level of the glucose tolerance test presented in Figure 1H.

Insulin Tolerance Test

Mice were fasted for 5 h before i.p. administration of insulin (1.0 U/kg body mass;) in normal saline. Blood glucose was measured at 0, 15, 30, 60, 90, and 120 after injection.

In Figure S1C, the fasting glucose level after 3 days of HFD feeding is derived from the baseline glucose level of the insulin tolerance test presented in Figure S1F.

Cold tolerance test

To determine the core body temperature response to an acute cold challenge, mice were single housed at 4°C without food and core body temperature was assessed via rectal probe every 60 min for 3 hours.

Hyperinsulinemic-Euglycemic Clamps

Carotid and jugular catheters were implanted into mice that had been fed HFD for 16 weeks to allow for sampling and infusion one week before the clamp study. During the recovery food intake and body weight was followed; mice were required to regain their pre-surgical body mass (±10%) to be included in the study. One week after catheter implantation mice were studied through a hyperinsulinemic-euglycemic clamps as described previously.[47,62] Two hours before infusions were started food was removed. To determine glucose fluxes, primed-continuous infusions of [U-^{13}C-6]-D-glucose (0.6 μmol/kg/min) were started at t = -100 min, at which time baseline plasma was collected, and the tracer infusions were continued until t = 120 min. Human insulin was primed (72 mU/ kg / min) at t = 0 min for 1 min and then continuously infused at 4 mU / kg / min for 2 hours. Blood glucose was monitored every 10 min, and a 20% dextrose solution was infused at a variable rate to maintain euglycemia. Blood was collected into EDTA tubes at multiple timepoints through tail nicks and processed for measuring plasma insulin and lipids. Animals were anesthetized with isoflurane and sacrificed at the end of the clamps. Perigonadal adipose tissues, livers, and hypothalamus were harvested, snap-frozen in liquid nitrogen, and stored at -80°C until further analysis.

Acute NE infusion

We sacrificed mice 15 min after i.p. injection of NE (4 mg/kg) and harvested eWAT.

Chronic NE infusion

Mice were implanted subcutaneously with osmotic minipumps (Alzet #1002, Durect Corporation, Cupertino, CA) delivering either NE; 5.0 mg/kg/day (Sigma #A7256, St. Louis, MO) or saline for 14 days.

Insulin signaling

To determine whether cellular insulin signaling is reduced during overnutrition, we sacrificed mice 15 min after i.p. injection of insulin (1 U/kg) and harvested tissues. Tissues were also harvested at the end of the hyperinsulinemic euglycemic clamp.

Please cite this article in press as: Sakamoto et al., Overnutrition causes insulin resistance and metabolic disorder through increased sympathetic nervous system activity, Cell Metabolism (2024), https://doi.org/10.1016/j.cmet.2024.09.012

2-DG Treatment

Mice were fasted for 5 hours before i.p. administration of 2-DG (500 mg/kg) dissolved in normal saline (Cat#: D6134; Sigma-Aldrich). Blood was collected from the tail vein at 0, 30, 60, 90 and 120 min after injection.

ATGListatin and NE treatment before Insulin tolerance test

To pharmacologically inhibit lipolysis, mice were gavage with corn oil or Atglistatin (S7364; Selleckchem) dissolved in corn oil (1.4 mg/Kg in a volume of 200 μl) 60 minutes before insulin tolerance test. The mice received either NE (0.5 mg/kg) or saline as vehicle through i.p. injection 15 minutes before insulin tolerance test.

CL 316,243 treatment

In the fed state, mice were i.p. injected with a bolus of the β3-adrenergic agonist CL 316,243 (CL, C5976 Sigma-Aldrich; i.p. 1 mg/kg body weight). Blood was collected from the tail vein at 0, 60, and 120 min after injection.

METHOD DETAILS

Western blot

Tissues were homogenized in lysed in ice-cold lysis buffer containing 50mM Tris-HCl pH 7.4, 150mM NaCl, 1mM EDTA, 1.25% CHAPS, 20 mM sodium fluoride, 1mM sodium orthovanadate, 10mM sodium pyrophosphate, 8mM β-glycerophosphate and Complete Protease Inhibitor Cocktail tablet (Roche, Indianapolis, IN). The homogenates were centrifuged at 14,000g for 15 minutes at −4 °C, and the supernatant was collected. Protein concentration was measured using a bicinchoninic acid (BCA) protein quantification kit (Thermo Scientific, Waltham, MA). Protein extracts were separated on 4–12% NuPAGE gels (Invitrogen, Carlsbad, CA) and blotted onto Immobilon FL PVDF membranes (Millipore, Billerica, MA). Membranes were blocked at room temperature for 1 h with Odyssey LI-COR blocking buffer (LI-COR, Lincoln, NE) diluted 1:1 in Tris-buffered saline (TBS). After blocking, membranes were incubated overnight at 4 °C with primary antibodies listed in the key resources table. Membranes were washed consecutively three times for 5 min each in TBS-T (0.1%). Blots were incubated with Dylight 680-conjugated goat anti–rabbit IgG and Dylight 800-conjugated goat anti–mouse IgG (Thermo Scientific, Waltham, MA) for 2 h at room temperature in blocking buffer containing 0.1% TBS-T and 0.1% SDS. Blots were washed three more times in TBS-T followed by a final wash in TBS, and the blots were then scanned with the LI-COR Odyssey (LI-COR, Lincoln, NE). Levels of phosphorylated proteins were normalized to the housekeeping genes β-actin or β-tubulin.

Preparation of RNA and gene-expression analysis

RNA Extraction and Quantitative Real-time PCR Total RNA from liver and adipose tissue was extracted and processed as previously described.[63] Briefly, homogenized tissue was processed using RNeasy Kit (Qiagen, Valencia, CA) to isolate RNA according to the manufacturer's protocol. The quantity and quality of the extracted RNA was assessed using SpectraMax i3x Multi-Mode Microplate Reader (Molecular Devices, San Jose, CA). cDNA was then synthesized using Superscript III Reverse Transcription Supermix; (Thermo Fisher Scientific, Waltham, MA) following the manufacturer's protocol. The resulting cDNA was used to determine gene expression levels via qPCR using SYBR green (Thermo Fisher Scientific, Waltham, MA). Relative gene expression was measured using the QuantStudio 6 Flex Real-Time PCR Systems (Thermo Fisher Scientific, Waltham, MA). Relative gene expression was calculated using the comparative Ct method. Data were analyzed with the comparative Ct method. The sequences of the quantitative real-time PCR primers are listed in the Table S1.

Hepatic TG Extraction

Folch TG extraction was performed as previously described.[64] Briefly, liver tissues (100 mg) were homogenized in a mixture of methanol and chloroform (1:2 ratio). After incubation, 0.1 mol/L NaCl was added to the homogenates, and samples were vortexed. After centrifugation at 1,000 rpm for 10 min at room temperature, the lower organic phase containing TGs was collected, and evaporated in a vacuum. 3 mol/L KOH was added to the extracted TGs, and the samples were incubated at 70°C for 1 h. TGs were measured using a triglyceride kit (Sigma Aldrich, St. Louis, MO) according to the manufacturer's protocol.

Histology

Fixed Liver and adipose tissue were embedded in paraffin and then sectioned at a thickness of 5 μm and stained with hematoxylin and eosin. Fixed adipose tissue were also stained with Masson's trichrome stain. Frozen liver samples were embedded in optimal cutting temperature compound (OCT, cat# 25608-930, VWR, Radnor, PA) and sectioned at a thickness of 5 μm. Slides were fixed and stained with an Oil Red O solution (ORO).

Slides were scanned with magnification of 10x, 20x and 40X using Olympus microscope and at least 4 images per animal were captured at 20x (adipocyte size measurement, Masson's trichrome staining) and 40x (oil red O staining) magnification. Percent and areas containing lipid or fibrillar collagens was calculated using Image J software.

The mean adipocyte weight was calculated as adipocyte volume multiplied by the density of TAG (0.915 g/ml) as described previously.[65] The total adipocyte number in eWAT was determined by dividing the total eWAT weight (milligrams) by the estimated mean adipocyte weight (milligrams).

Please cite this article in press as: Sakamoto et al., Overnutrition causes insulin resistance and metabolic disorder through increased sympathetic nervous system activity, Cell Metabolism (2024), https://doi.org/10.1016/j.cmet.2024.09.012

Plasma Assays

Plasma free-glycerol and TGs were measured with a colorimetric assay (Triglycerides Kit; Sigma-Aldrich, St. Louis, MO). NEFA levels and glycerol were determined using a NEFA kit from Wako (Wako Chemicals USA, Inc. Richmond, VA) and triglyceride determination kit from Sigma Aldrich (Sigma Aldrich, St. Louis, MO). Plasma insulin, Glucagon, Norepinephrine, Epinephrine, Corticosterone levels were determined using Ultrasensitive Mouse Insulin ELISA (Cat#: 10-1249-01, Mercodia, Sweden), Glucagon ELISA (Cat#: 10-1281-01, Mercodia, Sweden), Noradrenaline (Norpinephrine) High Sensitive ELISA (Cat#: NOU39-K01, Eagle Biosciences, NH, USA), Adrenaline (Epinephrine) High Sensitive ELISA (Cat#: ADU39-K01, Eagle Biosciences, NH, USA), Corticosterone Parameter Assay Kit (Cat#: KGE009, R&D systems, MN, USA). All assays were performed following the respective manufacturer's protocol.

Lipidomics analysis

UHPLC chromatography conditions: The reverse phase separation was performed on a Vanquish Horizon UHPLC system (Thermo Fisher Scientific, Waltham, MA) with a Poroshell 120 EC-C18 column (150 mm × 2.1 mm, 2.7 μm particle size, Agilent InfinityLab, Santa Clara, CA) using a gradient of solvent A (90%:10% H2O:MeOH with 34.2 mM acetic acid, 1 mM ammonium acetate, pH 9.4), and solvent B (75%:25% IPA:methanol with 34.2 mM acetic acid, 1 mM ammonium acetate, pH 9.4). The gradient was 0 min, 25% B; 2 min, 25% B; 5.5 min, 65% B; 12.5 min, 100% B; 19.5 min, 100% B; 20.0 min, 25% B; 30 min, 25% B. The flow rate was 200 μl/min. Injection volume was 5 μL and column temperature was 55 °C. The autosampler temperature was set to 4°C and the injection volume was 5μL.

Full scan mass spectrometry: The full scan mass spectrometry analysis was performed on a Thermo Q Exactive PLUS with a HESI source which was set to a spray voltage of -2.7kV under negative mode and 3.5kV under positive mode. The sheath, auxiliary, and sweep gas flow rates of 40, 10, and 2 (arbitrary unit) respectively. The capillary temperature was set to 300°C and aux gas heater was 360°C. The S-lens RF level was 45. The m/z scan range was set to 100 to 1200m/z under both positive and negative ionization mode. The AGC target was set to 1e6 and the maximum IT was 200ms. The resolution was set to 140,000.

BAT thermal imaging

BAT thermal imaging was performed as described previously.[66,67] Briefly, an infrared camera (T530, emissivity of 0.95, FLiR Systems) was placed above the mouse cage used to acquire a dorsal thermal video at a focal length of 30 cm, 3hours after cold exposure.

To analyze thermal images.CSQ video files were imported into the FLIR Tools+ program and the video was scrubbed through to find frames where mice were in a consistent and standardized outstretched position/orientation, allowing for clear delineation between the BAT heated interscapular region and relatively cooler hindquarters. Frames from the first three instances of mice in the standardized position were analyzed by drawing a region of interest (ROI) capturing the hindquarter region of the mouse and a second ROI capturing the BAT-containing interscapular region of the mice. The consistent mouse orientation allowed for identical sizing of the ROI boxes, which were sized at 46mm x 27mm.

For each mouse the mean of the warmest points of each ROI across the three frames was determined and used as the primary variable across conditions. The ratio of BAT/hindquarter temperature was calculated to normalize BAT temperature against general systemic heat generation and used as a proxy for relative BAT activity. Temperature scaling of representative thermal images was centered around the mean body temperature of all mice being compared and a scale span of 18 °C was used.

Inguinal and Gonadal SNA Recording

Male C57BL/6J mice were randomly assigned to RC or HFD for the next 16-weeks. For SNA recording, anesthesia was initially induced with 5% isoflurane and later sustained at 1-2% until the completion of the study. Each mouse was secured on its dorsal side, then a tapered micro-renathane tubing (MRE-40, Braintree Scientific) was inserted into the right jugular vein for volume infusion with sterile saline or injection of ketamine for end-point euthanasia. Another tapered MRE-40 catheter was inserted into the left carotid artery for continuous measurement of arterial pressure and heart rate. Core body temperature was monitored with a use of a rectal probe and continuously maintained at 37.5 °C with a temperature controller (Physitemp Model MCAT2).

To gain access to the nerve fascicle that innervates iWAT, a small skin incision was performed between the lower abdominal wall and the right flank just above the hindlimb. A single multi-fiber inguinal nerve embedded in the nearby white fat deposit, was isolated, placed on a bipolar platinum-iridium electrode (A-M Systems, 36-gauge) and secured with silicone gel (WPI, Kwik-Sil). The electrode was attached to a high-impedance probe (Grass Instruments, HIP-511) and the nerve signal was filtered at a 100- and 1000-Hz cutoff and amplified by 10^5 times with a Grass P511 AC pre-amplifier. The nerve signal was routed to a speaker system and to an oscilloscope (Hewlett-Packard, model 54501A) to monitor the audio and visual quality of the nerve recording. The nerve signal was also directed to a resetting voltage integrator (University of Iowa Bioengineering, model B600c) to analyze the total activity (integrated voltage) and finally to a MacLab analog-digital converter (ADInstruments, Castle Hill, New South Wales, Australia,Model 8S) containing the software (MacLab Chart Pro; Version 7.0) that utilizes a cursor to count the number of spikes/second that exceed the background noise threshold. Under a stable plane of anesthesia and strict isothermal conditions (37.5°C), continuous recording of baseline subcutaneous iWAT SNA was measured over a 30-minute basal period. At the end of the 30-min basal period, the inguinal nerve was sectioned, and background noise measured to normalize baseline inguinal nerve activity. After the completion of the nerve recording, the electrode was removed, and the skin incision closed with Vet-Bond.

Next, a small incision through the abdominal skin and muscle was made to access the interior pelvic area. The entire eWAT (right or left side) was carefully exteriorized and immediately encased in an oil-soaked gauze to protect the adipose tissue from exposure to

air. Under oil, the gonadal sympathetic nerve was carefully identified and separated from nearby vascular blood vessels at the base of the adipose tissue pad. A single multi-fiber gonadal nerve was placed on the same bipolar platinum-iridium electrode and secured with Kwik-Sil as before. Under a stable plane of anesthesia and strict isothermal conditions (37.5°C), continuous recording of baseline abdominal gonadal WAT SNA was measured over a 30-minute basal period. At the end of the 30-min basal period, the gonadal nerve was sectioned, and background noise measured to normalize baseline nerve activity.

QUANTIFICATION AND STATISTICAL ANALYSIS

Statistics

Data are expressed as the mean ± SEM. GraphPad Prism 6.0 software (GraphPad Software Inc., La Jolla, CA) was used for statistical analysis. When only two groups were analyzed, Student's unpaired t-test was performed to compare differences between the groups. To compare multiple groups, one-way ANOVA followed by Tukey's test was used. $P < 0.05$ was considered statistically significant.